Variable Fractional Order (VFO) PID Control for Precision Positioning

A Frequency Domain Approach

N. N. Nagda

Master of Science Thesis

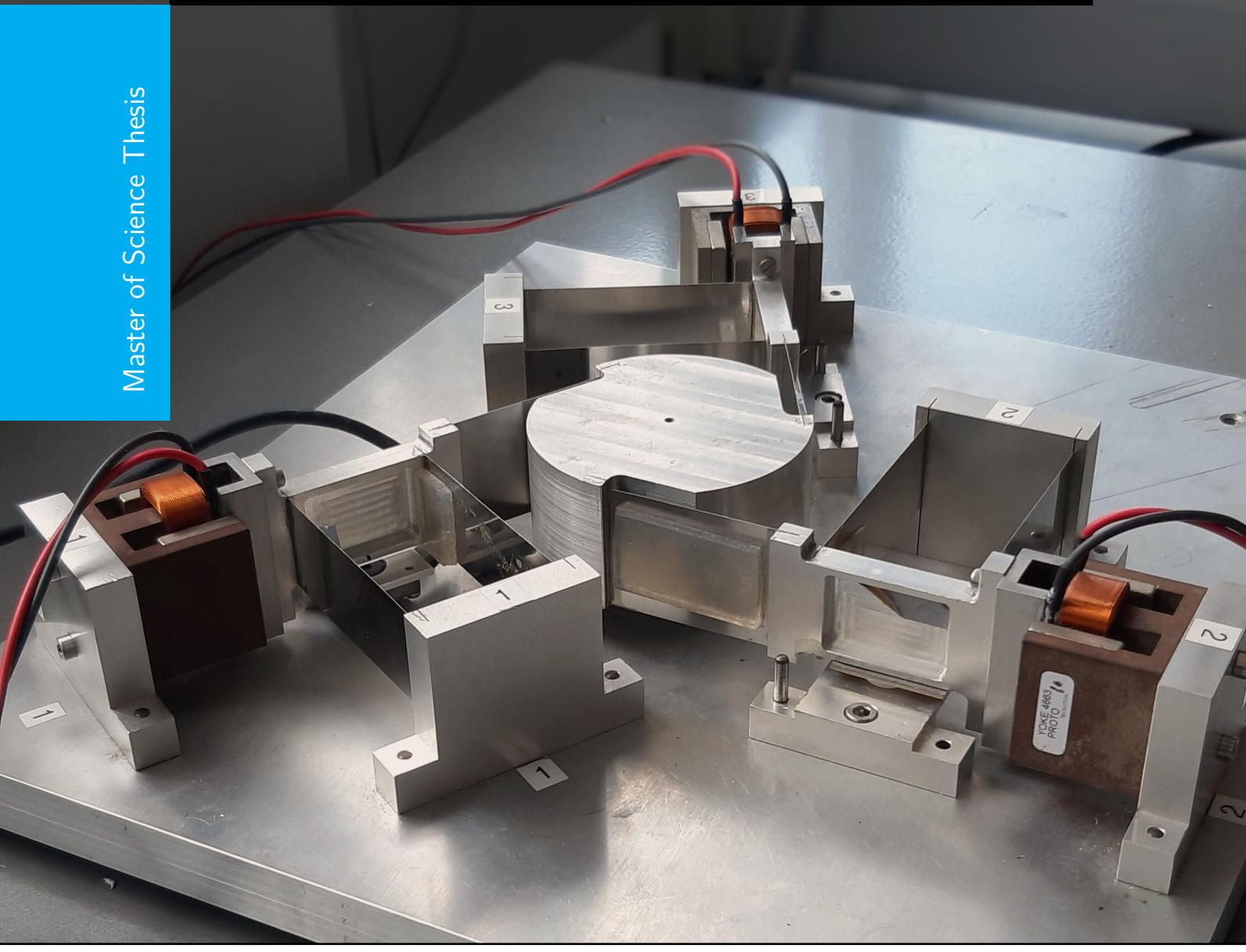

TU Delft Delft University of Technology

Delft Center for Systems and Control

Variable Fractional Order (VFO) PID Control for Precision Positioning

A Frequency Domain Approach

Master of Science Thesis

For the degree of Master of Science in Systems and Control at Delft University of Technology

N. N. Nagda

August 26, 2019

Student number:	4731913	
Thesis committee:	Prof.dr.ir. J.W. van Wingerden	DCSC, Chair
	Dr. G. Giordano	DCSC, Supervisor
	Dr. H. HosseinNia	PME, Supervisor
	Dr. N. Saikumar	PME, Daily Supervisor

Faculty of Mechanical, Maritime and Materials Engineering (3mE) · Delft University of Technology

Abstract

Stringent control demands from the high-tech mechatronics industry have warranted the need to explore potentially advantageous non-linear controllers. Variable Fractional Order (VFO) calculus provides one such avenue to build non-linear PID-like controllers. VFO calculus is the generalization of integer order differentiation and integration, where, in addition to the possibility of orders being real or even complex, the orders can vary as a function of a variable like time, temperature, etc. However, in this nascent field of VFO control, the focus has mainly been on controller tuning by time domain optimization of the performance for certain specific trajectories or cost functions. On the other hand, Frequency domain tools allow for analysis and tuning of controllers for performance over a wide range of exogenous inputs. For smooth adoption into industry, it is important to develop a frequency domain framework for working with VFO control. Describing function (DF) analysis is a method to obtain an approximate Frequency Response Function (FRF)-like function for non-linear systems. In this thesis, DF analysis is used for developing VFO PID controllers in the frequency domain from an industry compatibility point of view and the closed loop performance of these controllers in controlling a precision positioning stage is examined.

Table of Contents

Acknowledgements

The work presented in this thesis is the culmination of an amazing year-long journey filled with ups and downs, mistakes and learnings and loads of math and control. This story, however, shall be incomplete without expressing gratitude towards the heroes who fought by my side.

My daily supervisor **Niranjan Saikumar**. I can't thank you enough. Whenever I would meet you with weird looking plots, not knowing how to even start contemplating them, you always started the discussions with an encouranging "Interesting!". Thanks for all the critical discussions, guidance with the research and practical implementation and not to forget the lightening fast report reviews.

Hassan HosseinNia, my supervisor from PME. Firstly, thank you for offering me this amazing opportunity for working in the mechatronics design group on a project going beyond simulations. Moreover, thanks for the interesting remarks and monthly bouts of jollyness and positivity that made me feel good about my work after each controls' students meeting.

Giulia Giordano, my DCSC supervior. Thanks for coming in at critical points during the thesis and correcting my path. When I was feeling a bit lot in Jan, you asked me to start writing my literature survey right away, and writing helped me get clarity. Furthermore you went ahead and proposed my midterm date, which was crucial as it enabled me to maintain the thesis timeline.

Duarte Valerio, visiting professor from Técnico Lisboa. That one meeting at the very start of the project, debriefing me about Variable Fractional Order calculus got things rolling in the right direction for this project. Kudos!

Karst Brummelhuis, friend > colleague from DCSC, working with you on setting up the experiments, trying out different tweaks, cribbing about Labview coding, etc., all of it has been an absolute pleasure. Thanks for all the help and keep being "Curious!".

Bradley But, Rob Luttjeboer and Jos van Driel, the lab technicians. Thank you for the help in setting up the experiments.

Kudos to all my friends (read as family) here in Delft. On days when I was overjoyed with my results or on days when I felt hopeless as to where this thesis was going, they stood by me. Thanks Mihir, Nilay, Sukanya, Hussain, Sakina, Kaushal, Aditi and Reshma. Sribalaji and Sukrit, not just this thesis, but the MSc Systems and Control course would have been incomplete without you guys.

Lastly and most importantly, my backup stationed far away in another continent: Mijn ouders en mijn familie! Riche, dhelo, Path, Pachan, chachi, Akkudi, Neerudi, kaka, kaki, bai and everyone else. Thanks ammi and appa for believing in me and giving me this opportunity to pursue a Masters programme. Mom, you know me so well, you'd definitely make the perfect feedforward controller for me XD.

Have fun reading this thesis!

Delft, University of Technology N. N. Nagda
August 26, 2019

Eigen do it, if I try

- Jonathan Richard Shewchuk

Glossary

List of Acronyms

FO	Fractional Order
VFO	Variable Fractional Order
PID	Proportional-Integral-Derivative
SISO	Single Input Single Output
CRONE	Commande Robuste d'Ordre Non Entier
RL	Riemann-Liouville
GL	Grünwald-Letnikov
IAE	Integral of Absolute Error
ISE	Integral of Squared Error
ITAE	Integral of Time-weighted Absolute Error
ITSE	Integral of Time-weighted Squared Error
FRF	Frequency Response Function
GM	Gain Margin
PM	Phase Margin
MM	Modulus Margin
DF	Describing Function
SIDF	Sinusoidal Input Describing Function
TSIDF	Two Sinusoidal Input Describing Function
DIDF	Dual Input Describing Function

RIDF Random Input Describing Function

HOSIDF Higher Order Sinusoidal Input Describing Function

FFT Fast Fourier Transform

Notations

${}_0\mathscr{D}_T^{\alpha}$	Fractional Order (FO) operator of order α computed over the interval 0 to T $(T > 0)$
${}_0\mathscr{D}_T^{\alpha(t)}$	Variable Fractional Order (VFO) operator, where the varying order α is a function of time, computed over the interval 0 to T $(T > 0)$
$\binom{\alpha}{k}$	Binomial coefficient, i.e., α choose k
$\lvert \cdot \rvert$	Magnitude of the $\cdot$ complex number
$\angle \cdot$	Phase of the $\cdot$ complex number
$\mathbb{Z}^+$	Set of all positive Integers
$\mathbb{N}$	Set of all Natural numbers
$\mathbb{R}$	Set of all Real numbers
$\mathbb{R}^+ \backslash \mathbb{N}$	Set of all positive Real numbers minus the set of all Natural numbers
$\mathscr{L}$	Laplace transform operator
$\lfloor \cdot \rfloor$	the floor operator, i.e., rounds off $\cdot$ to the next integer smaller than $\cdot$
$\lceil \cdot \rceil$	the ceil operator, i.e., rounds off $\cdot$ to the next integer larger than $\cdot$
$\lVert \cdot \rVert_\infty$	L-Infinity Norm
$\lVert \cdot \rVert_2$	L-2 Norm

Chapter 1

Introduction

In this introductory chapter, the motivation for this thesis is presented, followed by an outline of this report.

1-1 Motivation

The high-tech mechatronics industry is constantly pushing for greater precision in motion control and faster production speeds for a range of applications [1–3] like lithography wafer scanners, atomic force microscopes (AFM)s, robotic manipulators, etc. These requirements of higher bandwidths and highly accurate reference tracking (in micro and even nanometres) warrant improvements in motion control techniques. Despite the advancements in feedback control theory, PID control, one of the earliest control techniques, still remains the preferred feedback controller in industry. This can be attributed to the intuitive underlying theory, simple structure, ease of analog as well as digital implementations, and years of research and practice giving rise to tried-and-tested rule-of-thumb tuning methods. Moreover, since PID controllers can be tuned using loop shaping techniques, they are compatible with frequency domain requirements and tools popular in industry.

But, PID controllers, being linear, are constrained by the fundamental limitations of linear feedback control[1] and this puts limitations on the achievable performance. Bode's gain phase relation and the sensitivity integrals (waterbed effect) [4, 5] give rise to inevitable trade-offs in controller tuning for performance objectives like low frequency reference tracking and disturbance rejection, and high frequency noise attenuation while maintaining stability and robustness margins.

Fractional Order (FO) calculus, which is the generalization of integer order differentiation and integration to arbitrary (non-integer) orders, i.e., rational, irrational or even complex orders, is as of late finding applications in modelling and control. Controllers built using FO calculus operators like Commande Robuste d'Ordre Non Entier (CRONE) [6] and $PI^{\lambda}D^{\mu}$ [7]

[1] A brief account on the limitations of linear feedback control can be found in A-3-1 and A-3-2.

are compatible with the PID framework, frequency domain tuning and provide greater tuning flexibility as compared to integer order controllers in tackling the above mentioned trade-offs. Despite these advantages, FO controllers are still linear and again the fundamental limitations limit the achievable performance.

Non-linear controllers, free from these fundamental limitations, are able to outperform linear controllers in several scenarios. However, most of them have complex tuning rules and esoteric literature, hindering their smooth adoption into industry. This motivates the development of non-linear controllers while remaining compatible with the widely-understood PID literature and frequency domain tools, to comply with industry standards. Quite a few non-linear controllers like SPAN filter [8], reset controllers built using Clegg integrator, Constant Gain Lead in phase (CGLP) element, first and second order reset elements [9–12], variable structure PID control [13], etc. fit this bill. The technique that enables analysis and tuning of these controllers in the frequency domain, is the Describing Function (DF) Analysis [14], which is a method to obtain an approximate Frequency Response Function (FRF)-like function for non-linear systems.

VFO calculus, introduced in 1998 by Lorenzo and Hartley [15], is the extension of the FO calculus, where the orders of derivative and integral operators are not only fractional but are also allowed to vary. VFO calculus is lately finding applications in modelling and control. It has been used to model viscous-viscoelastic damping in [16] and to model the bone remodelling process in a tumorous environment in [17]. As a natural extension of FO PID controllers, VFO PID controllers built using VFO calculus operators are being explored. A VFO PI controller where the order of the integrator switches based on the sign of the error is presented in [18]. The orders that the VFO integrator switches between and the controller gains K_p, K_i and are obtained by minimizing an Integral of Time-weighted Squared Error (ITSE) cost function. [19] explores a VFO PID ($PI^{\lambda(t)}D^{\mu(t)}$) controller where the orders of the VFO operators vary depending on the optimization objective chosen by a user or a higher level decision algorithm. Using particle swarm optimization to obtain the parameters of the VFO Proportional-Integral-Derivative (PID) controller for a Integral of Absolute Error (IAE) type objective function, has been proposed in [20]. But, much of the work that currently exists in VFO control, is focused on time domain controller tuning for optimized performance for specific trajectories or cost functions. On the other hand, frequency domain tools allow for analysis and tuning of controllers for performance over a wide range of exogenous inputs. For the smooth adoption into industry, it is important to develop a frequency domain framework for working with VFO control. To the best of our knowledge, no literature on VFO control in the frequency domain could be found and it is this gap that this research attempts to bridge. The goal of this thesis can thereby be stated as :

To use DF analysis for developing VFO PID controllers in the frequency domain from an industry compatibility point of view and examining their closed loop performance in a precision positioning application.

1-2 Outline

The flow of this thesis report is as follows. In chapters 2 and 3, a brief treatment on VFO calculus and DF analysis has been provided respectively. This is followed by defining the scope

of this research and laying down the objectives in chapter 4. Chapter 5 introduces the proposed VFO PID controller, followed by presenting its describing function analysis and frequency domain tuning guidelines. The closed loop performance of the developed controllers is tested on a precision positioning stage and the corresponding results are presented and discussed in Chapter 6. Chapter 7 puts forth the conclusions of this thesis and recommendations for future work.

Chapter 2

Variable Fractional Order (VFO) Calculus and Control

In this chapter, a brief introduction to Fractional Order (FO) calculus is given, building upto Variable Fractional Order (VFO) calculus. Post that, the relevant VFO definitions, implementation techniques and applications to control are presented.

2-1 Fractional Order (FO) calculus

Fractional calculus is the extension of integer order calculus that allows the orders to take rational, irrational or even complex values. An interesting characteristic of FO operators is their long memory of the input signal. Such memory, which is usually associated with integer order integrals, is not only possessed by FO integrals but derivatives as well. To illustrate this property, the Grünwald-Letnikov (GL)[1] definition of FO operators is presented here. Based on the generalization of the backward difference formula, the GL definition of the α^{th} order fractional derivative ($\mathscr{D}^{\alpha}$) of a function $f(t)$ in the interval $[0, T]$, computed at T, is given as:

$$ {}_0\mathscr{D}_T^{\alpha} f(t) = \lim_{h \to 0} \frac{1}{h^{\alpha}} \sum_{k=0}^{n} (-1)^k \binom{\alpha}{k} f(T - kh) \tag{2-1} $$

where,

- h is the sampling time step and $n = \lfloor T/h \rfloor$ is the number of samples in the interval $[0, T]$.
- $\binom{\alpha}{k}$ is the binomial coefficient, i.e., α choose k. $\binom{\alpha}{k} = \frac{\Gamma(\alpha+1)}{\Gamma(k+1)\Gamma(\alpha-k+1)}$

[1] Quite a few definitions exist for FO operators, but the most popular in literature being Riemann-Liouville (RL) and Grünwald-Letnikov (GL) definitions. A detailed treatment can be found in [6] and [21].

- Γ is Euler's Gamma function, which is the extension of the factorial function to accommodate real and complex numbers.

- $\alpha > 0$ implies fractional derivatives and $\alpha < 0$ implies fractional integrals.

It can be seen from Equation (2-1), that the computation of the fractional operator uses all the samples of the function being differentiated (over the interval under consideration), i.e., essentially it is not a local concept and demonstrates long memory characteristics. This is in contrast to the n^{th} integer order derivative that uses past values of function only upto the $f(T - nh)$ sample. This memory makes FO derivatives suitable for modelling certain phenomenon like anomalous diffusion, financial evolution, etc [22] and interesting for control applications [6, 7].

Furthermore, the Laplace transform of an α^{th} order fractional operator (for zero initial conditions) [21] is given as :

$$\mathscr{L}(\mathscr{D}^{\alpha} f(t)) = s^{\alpha} \mathscr{L}(f(t)) \tag{2-2}$$

and the corresponding FRF is

$$|(j\omega)^{\alpha}| = w^{\alpha} \qquad \angle (j\omega)^{\alpha} = \frac{\alpha\pi}{2} \tag{2-3}$$

Fig. 2-1 shows the frequency response of FO operators for different values of α.

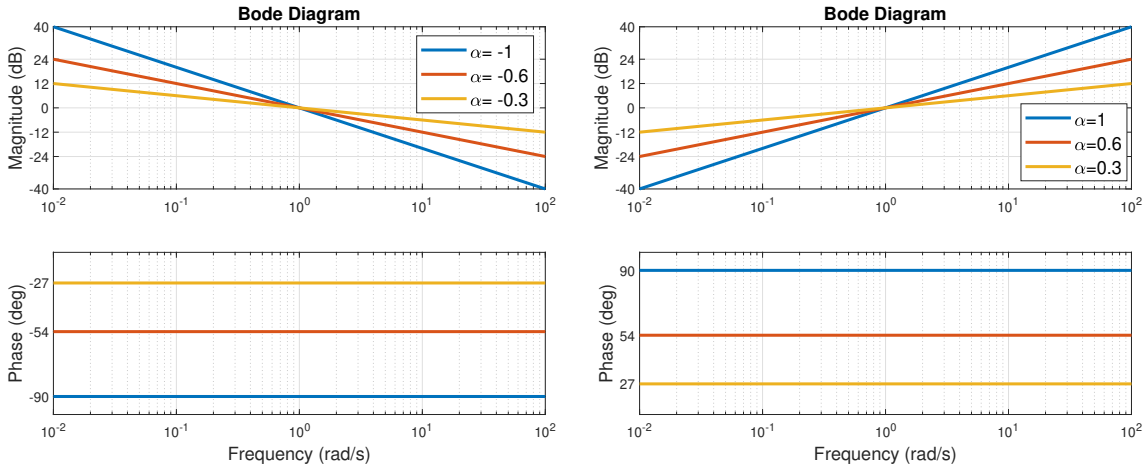

(a) Ideal frequency response of fractional integrals. **(b)** Ideal frequency response of fractional derivatives.

Figure 2-1: Ideal frequency response of fractional operators (s^{α}) for different values of α.

Such an FRF makes FO operators compatible with loop shaping techniques and the fact that α can take non-integer values empowers them with greater tunability as compared to integer order calculus operators. For further reading on FO calculus and control, the reader is referred to [6] and [21].

2-2 Variable Fractional Order (VFO) calculus

When the order of a FO operator varies as a function of the independent variable of integration/differentiation (eg. time) or some other variable like temperature, velocity, etc., it gives rise to a Variable Fractional Order (VFO) operator. This idea of extending FO calculus to accommodate varying orders was first proposed in 1998 by Lorenzo and Hartley [15]. This continuous order varying ability of VFO differential equations provides greater freedom in modelling certain dynamical systems as compared to using varying coefficients in constant integer order differential equations or piece-wise modelling. For example, the dynamics of a mass-spring-damper system can be modelled using an integer order differential equation as

$$m\mathscr{D}_t^2 x(t) + c\mathscr{D}_t^1 x(t) + kx(t) = F(t)$$

where m is the mass of the system, c is the damping coefficient, k is the stiffness and $\mathscr{D}_t^n$ is the n^{th} integer order time derivative operator. However, when the damping is viscous-viscoelastic, i.e., the damping force varies from pure viscous friction ($c\mathscr{D}_t^1 x(t)$) to pure viscoelastic friction ($c\mathscr{D}_t^{\frac{1}{2}} x(t)$) depending on the velocity, the damping force can be described by a VFO derivative as described in [16]. The previously presented equation of motion then becomes:

$$m\mathscr{D}_t^2 x(t) + c\mathscr{D}_t^{\alpha(\dot{x}(t))} x(t) + kx(t) = F(t)$$

where $\mathscr{D}_t^{\alpha(\dot{x}(t))}$ is the VFO derivative operator, where the order of differentiation varies with $\dot{x}(t) = \mathscr{D}_t^1 x(t)$ and can take non-integer values.

Other applications of VFO modelling include experimental study of an analogue realization of a temperature dependent VFO differentiator and integrator as presented in [23]. An application of VFO derivatives to model the bone remodeling process in a tumorous environment [17] led to simplification of the structure and compacter models as compared to the previously used integer order differential equations.

2-3 Definitions of VFO operators

VFO operator definitions are obtained by modifying the FO operator definitions to accommodate the varying nature of the order. The seminal paper by Lorenzo and Hartley [15] formally provided three definitions of VFO operators based on the Riemann-Liouville (RL) FO definition along with their equivalent parallel switching schemes, and introduced a metric for characterizing the memory of these operators.

Just like FO operators, VFO operators make use of the values of the input signal over the entire interval [0,T] over which they are being computed and hence have a memory of the input. This memory is termed as **m1**. The second type of memory corresponds to a memory of the history of the varying order of the operator. This is called **m2**. Depending on the definition, VFO operators possess m2 memory of varying degree. The order of a VFO operator, can vary continuously in value. However, for implementation as a switching system, this can be approximated by allowing the order to switch between a finite number of discrete values. Based on this notion, equivalent switching schemes have been developed for VFO definitions.

The corresponding VFO definitions based on the Grünwald-Letnikov (GL) and Caputo FO definitions have been presented in [24]. Furthermore, in the GL framework, 3 more definitions have been developed along with the corresponding serial switching schemes for all the 6 definitions by Sierociuk *et al.* [25–29]. No standard naming scheme exists for the VFO definitions and in this thesis, the nomenclature followed in the papers by Sierociuk *et al.* is used. In the following subsections, only two definitions that are used in this thesis are presented along with their equivalent parallel switching schemes.

2-3-1 Type $\mathcal{A}$

Modifying the FO GL definition (Equation (2-1)) such that the coefficients of all the function samples, $f(T-kh)$, are computed using $\alpha(T)$, i.e., the current value of α at the time when the VFO operator is being computed, the type $\mathcal{A}$ definition of VFO operators is obtained as :

$$ {}_0^{\mathcal{A}}\mathscr{D}_T^{\alpha(t)} f(t) = \lim_{h\to 0} \frac{1}{h^{\alpha(T)}} \sum_{k=0}^{n} (-1)^k \binom{\alpha(T)}{k} f(T-kh) \tag{2-4} $$

A VFO operator, thus defined, at any given point in time T when the operator is computed, behaves as if it had been operating with the current value of the order, $\alpha(T)$, from the very beginning of the interval and incorporates no memory of the past values of α. Thus it has no **m2** memory.

Equivalent Switching Scheme

The equivalent switching structure for type $\mathcal{A}$ VFO definition is presented in Fig. 2-2. Consider a VFO operator with a time varying order that switches between n constant FOs, α_j where $j \in \{1, 2, ..n\}$. The switching instances are given by t_j such that the order α_j is active in the time interval $\Delta t_j = [t_{j-1}, t_j)$ and $t_0 = 0 < t_1 < t_2 ... < t_n$. Depending on the current time T, the switches S_j, take positions a or b as follows:

$$ S_j = \begin{cases} b & \text{for } T \in \Delta t_j \\ a & \text{otherwise} \end{cases} \tag{2-5} $$

As can be seen from Fig. 2-2, the input $f(t)$ is being continuously fed into each of the individual FO operators ($\mathscr{D}^{\alpha_j}$) and as per the switching mechanism, the output y at time instance T will simply be the output of the FO operator corresponding to the order active at time T. Formally stating:

$$ y(T) = {}_0^{\mathcal{A}}\mathscr{D}_T^{\alpha(t)} f(t) = {}_0\mathscr{D}_T^{\alpha_j} f(t) \qquad \text{where } \{j \mid T \in \Delta t_j\} $$

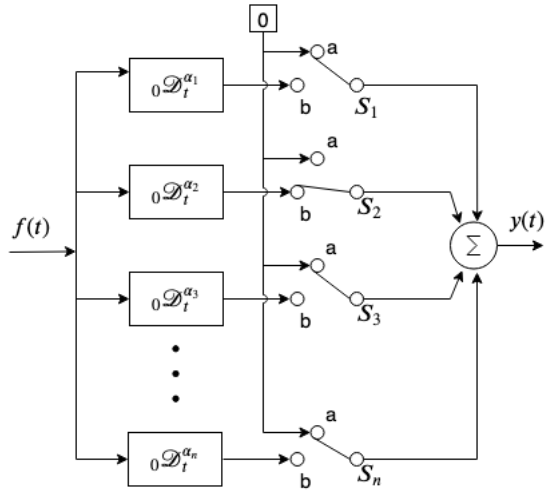

Figure 2-2: Equivalent switching scheme for type $\mathcal{A}$ VFO operator definition, where $f(t)$ is the input signal, $y(t)$ is the output, ${}_0\mathscr{D}_t^{\alpha_j}$ are FO operators and switches S_j are governed by the switching law (2-5). This particular combination of switch positions occurs when $t \in \Delta t_2$. Figure adapted from [15].

2-3-2 Type $\mathcal{B}$

Modifying Equation (2-1), such that the the coefficients of the function samples, $f(T-kh)$, are computed using $\alpha(T-kh)$, i.e., the coefficient of a past sample is computed using the corresponding value of α active at the time instance of that sample, the type $\mathcal{B}$ definition of VFO operators is obtained as :

$$ {}_0^{\mathcal{B}}\mathscr{D}_T^{\alpha(t)} f(t) = \lim_{h\to 0} \sum_{k=0}^{n} \frac{(-1)^k}{h^{\alpha(T-kh)}} \binom{\alpha(T-kh)}{k} f(T-kh) \tag{2-6} $$

A VFO operator, thus defined, unlike type $\mathcal{A}$ VFO definition, uses the past values of α for computation and hence possesses memory of the order history. However, memory of the oldest orders becomes weaker as the interval $[0,T]$ becomes longer.

Equivalent Switching Scheme

The equivalent switching structure for type $\mathcal{B}$ VFO definition is presented in Fig. 2-3. Again, consider a VFO operator with a time varying order that switches between n constant FOs, α_j where $j \in \{1,2,..n\}$. The switching instances are given by t_j such that the order α_j is active in the time interval $\Delta t_j = [t_{j-1}, t_j)$ and $t_0 = 0 < t_1 < t_2 ... < t_n$. The switches are governed by the law in Equation 2-5.

As can be seen from Fig. 2-3, each FO operator ${}_0\mathscr{D}_t^{\alpha_j}$ receives $f(t)$ as the input when $t \in \Delta t_j$ and 0 otherwise. The input received by ${}_0\mathscr{D}_t^{\alpha_j}$ can be written in terms of two delayed step functions ($U(t)$) as

$$ f(t)\big(U(t-t_{j-1}) - U(t-t_j)\big) $$

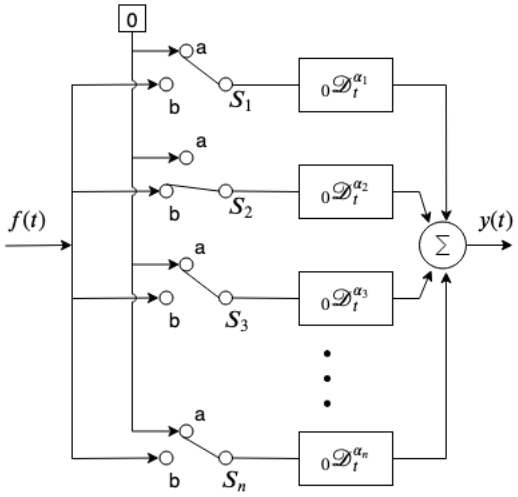

Figure 2-3: Equivalent switching scheme for type $\mathcal{B}$ VFO operator definition, where $f(t)$ is the input signal, $y(t)$ is the output, ${}_0\mathscr{D}_t^{\alpha_j}$ are FO operators and switches S_j are governed by the switching law (2-5). This particular combination of switch positions occurs when $t \in \Delta t_2$. Figure adapted from [15].

And the output y of the VFO operator, at any instance T, is the sum of the outputs of all individual FO operators at that instance. This can be formally stated as :

$$\begin{aligned} y(T) &= {}_0^{\mathcal{B}}\mathscr{D}_T^{\alpha(t)} f(t) \\ &= \sum_{j=1}^{n} {}_0\mathscr{D}_T^{\alpha_j}\big[f(t)\big(U(t-t_{j-1}) - U(t-t_j)\big)\big] \end{aligned}$$

To sum it up, in type $\mathcal{A}$ definition, all the FO operators constantly receive the VFO operator input and the switching scheme governs which FO operator's output contributes to the VFO operator output while the other operators contribute 0. In type $\mathcal{B}$ definition, the switching governs which FO operator receives the VFO operator input while the other operators receive 0, and the VFO operator output is the sum of the outputs of all FO operators.

2-4 Implementation techniques

In this thesis, the VFO operators are implemented using the equivalent parallel switching schemes introduced in [15] and demonstrated here in Fig. 2-2 and 2-3. This choice is made due to their intuitiveness and simplicity as compared to other techniques. To put this into perspective, the other implementation methods found in literature are presented here :

- **Discrete time implementation using the GL VFO definitions**. This can be done using the Matlab toolbox developed by Sierociuk *et al.* [30]. As the VFO operator makes use of all the past samples of its input, the number of samples to be stored and the computations required to calculate the VFO operator will go on increasing as the

duration of the experiment increases. It is ideal if samples from the entire duration of the experiment can be stored and used, but in the cases when this is not possible due to finite storage and computation power, older data needs to be discarded. The toolbox tackles this issue by limiting the number of past samples to be stored and used for computing the VFO operator, to a finite user-defined variable. To what extent, this truncation affects the output has not been fully analysed. Another problem with this implementation is that, the $\Gamma(k+1)$ present in the denominator of the operator definition blows to infinity for a comparitively small finite value , eg. k= 171 in Matlab, hence the samples beyond this in the past essentially have zero weights, which is as good as truncation[2].

- **Discrete time implementation using the RL and Caputo VFO definitions** can be achieved by approximating derivatives in the definitions with finite differences and integrals with trapezoidal numerical integration [31].
- **Analog circuits** based on the equivalent series switching schemes of the GL VFO definitions, as presented in the work by Sierociuk *et al.* [25–29].
- **VFO operator representation by fuzzy logic and polynomial interpolation between FO operators** [31]. This method implements VFO operators with orders varying between $[-1, 1]$ by first considering a finite number of FO operators with orders in $[-1, 1]$ approximated using Oustaloup approximation [32] and discretized using Tustin's method. The VFO operator is then represented as an interpolation between these FO operators, using fuzzy logic. By changing the fuzzy inference engines, different **m2** characteristics of the VFO operator can be obtained.

2-5 Applications to control

In this section, a few applications of VFO calculus in control are described to present the state of the art and more importantly, to emphasize on the fact that current work primarily focuses on time-domain tuning.

- In [19], the idea of VFO Proportional-Integral-Derivative (PID), i.e., $PI^{\lambda(t)}D^{\mu(t)}$, where the fractional orders of the operators vary depending on the optimization objective chosen has been presented. The 3 controller gains (K_p, K_i and K_d) are obtained by Ziegler Nichols method and then the $\lambda(t)$ and $\mu(t)$ are obtained by Integral of Absolute Error (IAE) or Integral of Time-weighted Absolute Error (ITAE) optimization, either of which may be chosen by the user or higher level decision algorithm. In the numerical simulations of closed loop step responses of a 2^{nd} order plant controlled by the VFO PID, the switching instances of the optimization objective function, and there by the order switching instances, have been chosen arbitrarily and a comparison has been made between implementations of the VFO PID based on the type $\mathcal{A}$ and type $\mathcal{B}$ definitions.
- [18] presents a VFO PI controller for a 2^{nd} order plant, where the order of the integral switches based on the sign of the error. Type $\mathcal{A}$, $\mathcal{B}$, $\mathcal{D}$ and $\mathcal{E}$ definitions are considered

[2] A workaround has been suggested in [31].

for implementing the VFO integrator. The orders α_1 and α_2, that the VFO integrator switches between and the controller gains K_p, K_i are obtained by minimizing an Integral of Time-weighted Squared Error (ITSE) cost function using the fmincon function from Matlab. Numerical simulations are performed using the toolbox by Sierociuk *et al.* [30]. For the with and without actuator saturation cases, a comparative study of the performance of an integer order PI, a FO PI and VFO PI controllers is made based on rise time, settling time, overshoot, peak time and the minimal cost achieved for ITSE objective function.

- [33] approaches the problem of growing calculation tail and stability of the closed loop with a VFO PID controller by initially allowing the order of I-action and D-action (λ and μ respectively) to be fractional and vary as a function of tracking error, controller output or both and then pushing λ to -1 and μ to 1, i.e., making the VFO PID a standard integer order PID, after a certain number of samples. The authors propose obtaining the gains of the PID controller using IAE or Integral of Squared Error (ISE) optimization.

- [20] proposes the Using particle swarm optimization to obtain the parameters of the VFO PID for a IAE type objective function. Numerical simulations have been provided comparing the performance of Integer Order PID, FO PID and Type $\mathcal{A}$ and type $\mathcal{B}$ definition based VFO PID for 3 different systems. VFO controllers were found to be beneficial for plants with time varying coefficients.

Chapter 3

Describing Function Analysis

This chapter provides the necessary background on describing function analysis that will be used for analysis and tuning of the proposed VFO controllers. Firstly, the basic idea behind describing function analysis is introduced in section 3-1, followed by discussing Sinusoidal Input Describing Function (SIDF) in section 3-2 and lastly explaining Higher Order Sinusoidal Input Describing Function (HOSIDF) in section 3-3.

3-1 Introduction

Frequency domain tools like Bode and Nyquist plots play a crucial role in loop shaping since they provide useful visual information about the closed loop stability and performance of linear systems over the entire range of frequencies. These tools make use of the Frequency Response Function (FRF) of the system which gives the input-output relation of the system as a function of the input frequency. The usual method adopted for working with non-linear systems, is to linearize the system about an operating point and then study the FRF of this linearization. However, there exists another way of analysing non-linear systems in an FRF-like fashion, called the Describing Function (DF) analysis [14]. The underlying idea is to approximate the periodic output of a non-linear system (for a sinusoidal input), by only the first harmonic content in the output and then use this information to obtain an FRF-like function which gives the gain and phase characteristics of the non-linear system as a function of input frequency and amplitude. DF is denoted by $N(A, \omega)$. A block representation of this idea can be seen in Figure 3-1.

The basic version DF method requires the non-linear system to satisfy the following conditions [14]:

- There must be **only one non-linear element in the system**. If there are more than one, then either they they must be lumped together or only the primary non-linearity must be considered.

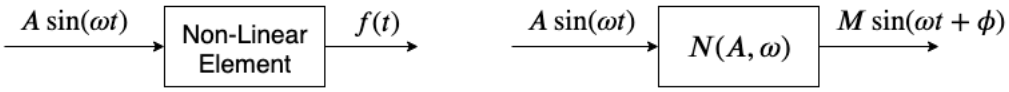

Figure 3-1: Block diagram representation of a non-linear element on the left and the corresponding DF approximation on the right, where $A\sin(\omega t)$ is the input to the non-linearity and $M\sin(\omega t + \phi)$ is the first harmonic content in the output $f(t)$. Figure adapted from [14].

- The **non-linear element must be time invariant**. Just like the FRF, DF method can be applied only to time invariant non-linearities.
- The **linear element in series with the non-linear element must have low pass filtering characteristics**. Only then can the higher order harmonics be neglected. This is the filtering hypothesis.

As newer methods of DF analysis were developed namely Two Sinusoidal Input Describing Function (TSIDF), Dual Input Describing Function (DIDF), Random Input Describing Function (RIDF) [34] and Higher Order Sinusoidal Input Describing Function (HOSIDF) [35], the basic version of DF described here, came to be known as Sinusoidal Input Describing Function (SIDF).

3-2 Sinusoidal Input Describing Function (SIDF)

The SIDF is essentially a Fourier series approximation of the non-linear system output where only the first harmonic information is retiained. The Fourier series approximation, $f_{FS}(t)$ of a periodic function of time, $f(t)$ periodic with time period T and frequency ω is given by

$$\begin{aligned} f_{FS}(t) =& \frac{a_0}{2} + \sum_{n=1}^{\infty} \left[a_n \cos(n\omega t) + b_n \sin(n\omega t) \right] \\ a_n =& \frac{2}{T} \int_0^T f(t) \cos(n\omega t) dt \\ b_n =& \frac{2}{T} \int_0^T f(t) \sin(n\omega t) dt \end{aligned}$$

If only the first harmonic is considered, the following is obtained :

$$\begin{aligned} f_{1h}(t) =& a_1 \cos(\omega t) + b_1 \sin(\omega t) \\ =& \sqrt{a_1^2 + b_1^2} \sin(\omega t + \tan^{-1}\left(\frac{a_1}{b_1}\right)) \\ =& M \sin(\omega t + \phi) \end{aligned}$$

For a sinusoidal input of amplitude A and frequency ω, the SIDF of the non-linear system is defined as the the complex ratio of the first harmonic component in the output $f(t)$, to the input sinusoid.

$$N(A,\omega) = \frac{M\sin(\omega t+\phi)}{A\sin(\omega t)} = \underbrace{\frac{Me^{j(\omega t+\phi)}}{Ae^{j\omega t}}}_{\text{Phasor representation}} = \frac{b_1 + ja_1}{A}$$

The real and imaginary parts of SIDF are thus given by:

$$\begin{aligned} Re(N(A,\omega)) &= \frac{2}{TA}\int_0^T f(t)\sin(\omega t)dt \\ Im(N(A,\omega)) &= \frac{2}{TA}\int_0^T f(t)\cos(\omega t)dt \end{aligned} \tag{3-1}$$

Some additional pointers about SIDF analysis :

- Besides approximating the input output relationship[1] for the non-linear system in frequency domain, SIDF is used for limit cycle analysis.
- When the non-linearity is single valued, i.e., the output has only one value for a given input (unlike hysterisis) then the SIDF is independent of the frequency.
- When the non-linearity is odd, the SIDF is real, since the coefficient of the cosine term (a_1) will be zero.

SIDF analysis has been used in analysis and tuning of non-linear controllers like reset controllers [9–12], variable structure PID control [13], etc.

3-3 Higher Order Sinusoidal Input Describing Function (HOSIDF)

As seen in the previous section, SIDF gives the gain and phase relation between a sinusoid input and the first harmonic content in the corresponding periodic response of a non-linear system. However, for precision applications where the specifications are stringent, the higher harmonic content in the output of the non-linearity cannot be neglected as it would deteriorate performance. Also, when the output contains discontinuities, jumps, etc., it is not well-approximated by a single sinusoid and higher harmonics information must also be taken into account. HOSIDF is the extension of the SIDF technique, such that it takes higher harmonic content information into account as well. The n^{th} order HOSIDFs, denoted by $H_n(A,\omega)$, relate the magnitude and phase of the n^{th} harmonic content in the output to the magnitude and phase of a sinusoidal input [35], [36]. An important notion introduced in the HOSIDF literature is that of a virtual harmonics generator, which is a block which takes in a sinusoidal input, and generates higher harmonics as shown in Fig. 3-2.

Now, as per the HOSIDF technique, a non-linear system with sinusoidal excitation (Fig. 3-3) can be approximated by a block consisting of a virtual harmonics generator, SIDF ($N(A,\omega)$) and n HOSIDFs ($H_n(A,\omega)$) as shown in Fig. 3-4.

[1] Since the superposition principle does not hold for non-linear systems and since SIDF is an approximation in the first place, the SIDF is not as effective as FRF is for linear systems.

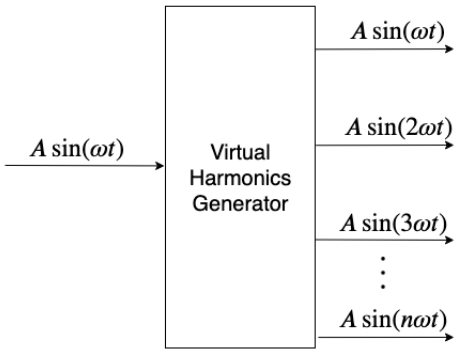

Figure 3-2: Virtual Harmonics Generator. Figure adapted from [35].

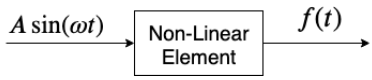

Figure 3-3: A non-linear element with a sinusoidal excitation $A\sin(\omega t)$ and output $f(t)$.

If we take the n^{th} harmonic content from the Fourier series approximation of $f(t)$, we get

$$\begin{aligned} f_{nh}(t) =& a_n \cos(n\omega t) + b_n \sin(n\omega t) \\ =& \sqrt{a_n^2 + b_n^2} \sin(n\omega t + \tan^{-1}\left(\frac{a_n}{b_n}\right)) \\ =& M_n \sin(n\omega t + \phi_n) \end{aligned}$$

$H_n(A,\omega)$ can then be obtained as the the complex ratio of the n^{th} harmonic component in the output $f(t)$ to the n^{th} harmonic of the input sinusoid.

$$H_n(A,\omega) = \frac{M_n \sin(n\omega t + \phi_n)}{A\sin(n\omega t)} = \underbrace{\frac{M_n e^{j(n\omega t + \phi_n)}}{A e^{jn\omega t}}}_{\text{Phasor representation}} = \frac{b_n + j a_n}{A}$$

Thus we obtain $H_n(A,\omega)$ in terms of the the Fourier coefficients of the n^{th} harmonic in the non-linear element output. There are 2 methods to obtain the HOSIDFs numerically, namely IQ (in-phase/quadrature-phase) demodulation and Fast Fourier Transform (FFT)-based. These methods are discussed in detail in [35] along with the applications of these methods for obtaining HOSIDFs for backlash and a mechanical system with friction. The use of HOSIDF analysis in the field of reset control design can be found in the work by 'Mechatronic System Design' group at the PME department of TU Delft [37–39].

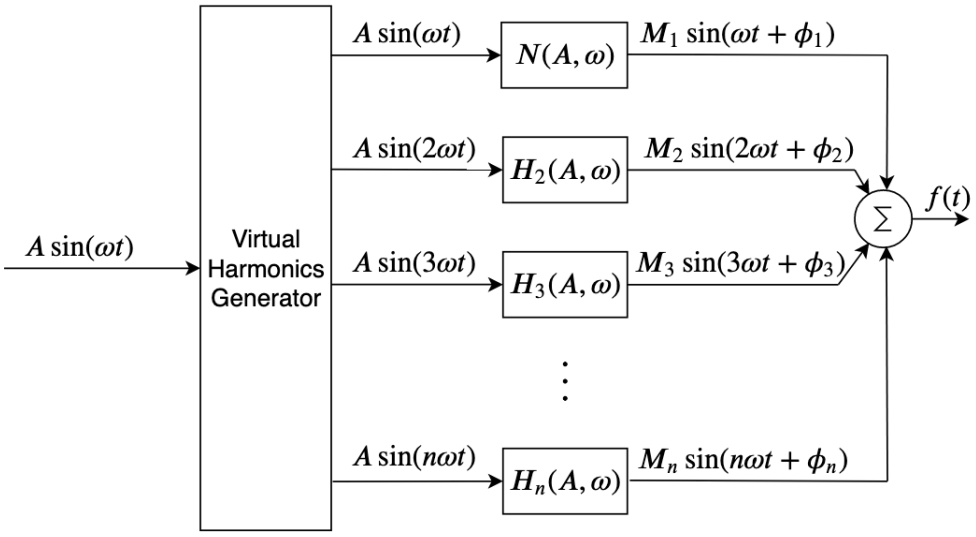

Figure 3-4: The HOSIDF approximation of the non-linear element (Fig. 3-3), where $N(A,\omega)$ is the SIDF and $H_n(A,\omega)$ is the n^{th} order HOSIDF. Figure adapted from [35].

Chapter 4

Research Objectives

Now that the necessary background needed for understanding the development of the VFO PID controller is established, this chapter defines the scope of this research and lays down the objectives to be achieved.

4-1 Scope

- **Definitions:** A VFO operator can be realised in different ways depending on the definition used. Although, many definitions exist for VFO operators, given the limited time frame of this thesis, only 2 definitions are explored. Type $\mathcal{A}$ and type $\mathcal{B}$ definitions have been chosen since they provide contrasting order memory characteristics, i.e., type $\mathcal{A}$ does not possess **m2** memory while type $\mathcal{B}$ does.
- **Implementation:** Moreover the choice to implement the VFO operators using their equivalent parallel switching schemes Fig. 2-2, 2-3 has been made since they are intuitive to understand, simpler to implement and easier to derive describing functions for.
- **Order signal** ($\alpha(t)$)**:** The order signal is defined as a switching signal, switching between only 2 orders α_1 and α_2, based on a switching law. The reason for switching between only two orders is that the chosen switching law, presented in the next chapter, allows for switching between two orders only. Since this is a preliminary study, the scope is limited to $\alpha_1, \alpha_2 \in$ {-1,0,1} only, i.e., P, I or D operators only. This gives rise to 6 order combinations {D-I, P-I, D-P, I-D, I-P, P-D} each for type $\mathcal{A}$ and type $\mathcal{B}$ VFO operators, to be investigated.

4-2 Objectives

1. Obtain the SIDFs for the 6 cases of type $\mathcal{A}$ VFO operator. These SIDFs are obtained from the SIDF of the Variable Structure PID controller [13].

2. Building up on this work, derive the HOSIDFs for these 6 cases and the SIDF and HOSIDFs for the 6 cases of type $\mathcal{B}$ VFO operator.

3. Analyse the SIDFs to shortlist the order combinations to be further used to build the VFO controllers.

4. Tune the VFO controllers using loop shaping guidelines.

5. Implement the controllers on a precision positioning stage and examine the closed loop performance.

Chapter 5

Frequency Analysis and Tuning of VFO Controller

This chapter delineates the process of building Variable Fractional Order (VFO) PID controllers. Firstly, the structure of the proposed VFO controller is explained, followed by the derivation and analysis of the describing functions for the required VFO operators. Lastly, the frequency domain tuning guidelines for the VFO PID controllers are presented.

5-1 Proposed VFO controller

The proposed VFO controller comprises of a VFO operator ($\mathscr{D}^{\alpha(t)}$) in series with a linear filter as depicted in Fig. 5-1.

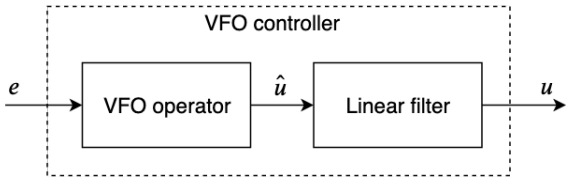

Figure 5-1: Block diagram of the proposed VFO controller, where e is the tracking error, $\hat{u}$ is the VFO operator output and u is the generated control input.

As mentioned in Section 4-1, the scope of this thesis is limited to the type $\mathcal{A}$ and type $\mathcal{B}$ VFO operators only. These operators are implemented as switching systems using their respective equivalent parallel switching schemes (Fig. 2-2 and 2-3 respectively). Further narrowing the scope of investigation, the order signal $\alpha(t)$ is designed such that it switches between only two discrete values, α_1 and α_2, based on a switching law. Such a type $\mathcal{A}$ VFO operator, denoted as ${}^{\mathcal{A}}\mathscr{D}^{\alpha_1-\alpha_2}$, is shown in Fig. 5-2.

In Fig. 5-2, $\mathscr{D}^{\alpha_1}$ and $\mathscr{D}^{\alpha_2}$ are two FO operators, and as a modification to the type $\mathcal{A}$ switching scheme in Fig. 2-2, gains K_1 and K_2 for these FO operators have been additionally

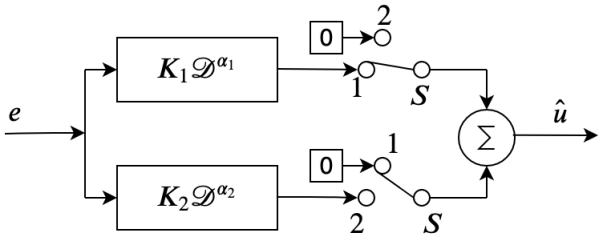

Figure 5-2: Type $\mathcal{A}$ VFO operator (${}^{\mathcal{A}}\mathscr{D}^{\alpha_1-\alpha_2}$).

incorporated. Both these operators are constantly receiving the input e. When the switches S take position 1, the VFO operator has order α_1 and the output $\hat{u}$ is simply the output of $K_1\mathscr{D}^{\alpha_1}$ while $K_2\mathscr{D}^{\alpha_2}$ contributes 0 and vice versa for when S takes position 2. Similarly, the type $\mathcal{B}$ VFO operator (${}^{\mathcal{B}}\mathscr{D}^{\alpha_1-\alpha_2}$) is implemented as shown in Fig. 5-3.

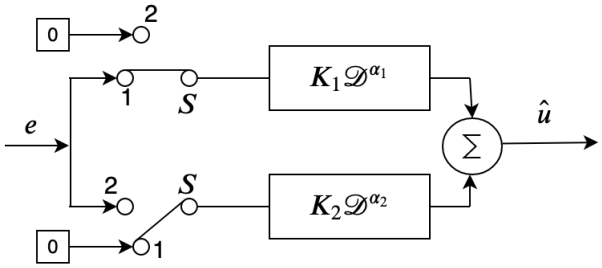

Figure 5-3: Type $\mathcal{B}$ VFO operator (${}^{\mathcal{B}}\mathscr{D}^{\alpha_1-\alpha_2}$).

Here, when S takes position 1, only $K_1\mathscr{D}^{\alpha_1}$ receives the input while $K_2\mathscr{D}^{\alpha_2}$ receives 0 and vice versa for when S takes position 2. The output $\hat{u}$, at any instance, is the sum of outputs of the individual FO operators.

The switches S in these switching schemes are governed by the following switching law :

$$S = \begin{cases} 1 & \text{for } sgn(e\dot{e}) > 0 \\ 2 & \text{for } sgn(e\dot{e}) \leq 0 \end{cases} \tag{5-1}$$

where e is the tracking error[1], i.e., reference signal minus the measured output and $\dot{e}$ is the derivative of the tracking error. When the error is increasing in magnitude, i.e., $sgn(e\dot{e}) > 0$ the order of VFO operator is α_1 while when the error is non-increasing, i.e., $sgn(e\dot{e}) \leq 0$, the order is α_2. Such a switching law has also been used in a paper on Variable structure PID control [13], where it is used for switching between two PID controllers.

As specified in the scope (Section 4-1), the orders are chosen such that $\alpha_1, \alpha_2 \in \{-1, 0, 1\}$, i.e., the operators in either branch of these switching schemes can be I, P or D blocks only. Henceforth, in the notations used for these operators, the superscript to the left denotes the type of definition and the superscript to the right denotes the orders $\alpha_1 - \alpha_2$. For example, ${}^{\mathcal{A}}\mathscr{D}^{P-I}$, represents a type $\mathcal{A}$ VFO operator with order switching between $\alpha_1 = 0$ and $\alpha_2 = -1$.

[1]The terminology is with reference to a negative feedback control loop (Fig.A-1).

Next, the Sinusoidal Input Describing Function (SIDF) and Higher Order Sinusoidal Input Describing Function (HOSIDF) for these VFO operators are derived.

5-2 Type $\mathcal{A}$ VFO operator SIDF

Instead of obtaining an individual SIDF for each of the 6 cases, the SIDF for a switching system as depicted in Fig. 5-4 is obtained. This is a type $\mathcal{A}$ switching scheme, but instead of switching between just two operators, it switches between two distinct PID controllers with gains K_{pj}, K_{ij}, K_{dj} with $j \in 1, 2$ and the switches S governed by the switching law in Equation (5-1). The idea is to obtain the required SIDFs of the 6 combinations by setting the appropriate PID gains to 0 in the SIDF derived for this system. This system is called a variable structure PID controller and the SIDF for it has been derived in [13]. The derivation is being presented here to elucidate the steps involved, so it will help the reader to follow along as this thesis builds up on this work to derive the HOSIDFs for type $\mathcal{A}$ and the SIDF and HOSIDFs for type $\mathcal{B}$ operators.

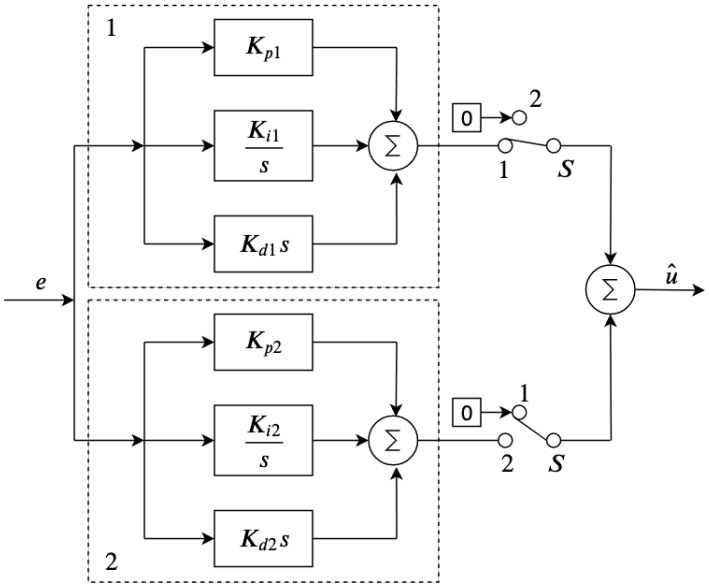

Figure 5-4: Type $\mathcal{A}$ switching scheme, switching between two PID controllers instead of just two FO operators. This scheme is known as Variable structure PID controller [13].

For an input $e = Asin(\omega t)$, the real and imaginary parts of the SIDF for this system are given as :

$$\begin{aligned} Re({}^{\mathcal{A}}N^{PID-PID}(A,\omega)) &= \frac{2}{TA}\int_0^T \hat{u}(t)\sin(\omega t)dt \\ Im({}^{\mathcal{A}}N^{PID-PID}(A,\omega)) &= \frac{2}{TA}\int_0^T \hat{u}(t)\cos(\omega t)dt \end{aligned} \tag{5-2}$$

Over one time period T of the input sinusoid, the switching signal behaves as :

$$e\dot{e} = \begin{cases} > 0 & \text{in } [0, \frac{T}{4}] \\ \leq 0 & \text{in } [\frac{T}{4}, \frac{T}{2}] \\ > 0 & \text{in } [\frac{T}{2}, \frac{3T}{4}] \\ \leq 0 & \text{in } [\frac{3T}{4}, T] \end{cases} \tag{5-3}$$

And owing to the corresponding switching, the output $\hat{u}$ is :

$$\hat{u} = \begin{cases} \overbrace{K_{p1}A\sin(\omega t)}^{P} + \overbrace{\frac{1}{\omega}K_{i1}A\big[1-\cos(\omega t)\big]}^{I} + \overbrace{\omega K_{d1}A\cos(\omega t)}^{D} & \text{for } t \in [0, \frac{T}{4}] \\ K_{p2}A\sin(\omega t) + \frac{1}{\omega}K_{i2}A\big[1-\cos(\omega t)\big] + \omega K_{d2}A\cos(\omega t) & \text{for } t \in [\frac{T}{4}, \frac{T}{2}] \\ K_{p1}A\sin(\omega t) + \frac{1}{\omega}K_{i1}A\big[1-\cos(\omega t)\big] + \omega K_{d1}A\cos(\omega t) & \text{for } t \in [\frac{T}{2}, \frac{3T}{4}] \\ K_{p2}A\sin(\omega t) + \frac{1}{\omega}K_{i2}A\big[1-\cos(\omega t)\big] + \omega K_{d2}A\cos(\omega t) & \text{for } t \in [\frac{3T}{4}, T] \end{cases} \tag{5-4}$$

Where the overbrace notations denote the outputs of P, I and D operators of either controllers. Solving Equation (5-2) for the $\hat{u}$ from Equation (5-4), we get

$$\begin{aligned} &{}^{\mathcal{A}}N^{PID-PID}(\omega) = \\ &\left[\left(\frac{K_{p1}+K_{p2}}{2}\right) + \frac{-1}{\omega}\left(\frac{K_{i1}-K_{i2}}{\pi}\right) + \omega\left(\frac{K_{d1}-K_{d2}}{\pi}\right)\right] \\ &+ j\left[\left(\frac{K_{p1}-K_{p2}}{\pi}\right) + \frac{-1}{\omega}\left(\frac{K_{i1}+K_{i2}}{2}\right) + \omega\left(\frac{K_{d1}+K_{d2}}{2}\right)\right] \end{aligned} \tag{5-5}$$

It is observed that this SIDF is independent of the amplitude of the applied sinusoid, and only a function of its frequency. From Equation (5-5), we can obtain, for example, the ${}^{\mathcal{A}}N^{P-D}$ SIDF by plugging in $K_{p1} = K_1$ and $K_{d2} = K_2$ and all the other gains to 0, giving us:

$${}^{\mathcal{A}}N^{P-D} = \left[\frac{K_1}{2} - \omega\frac{K_2}{\pi}\right] + j\left[\frac{K_1}{\pi} + \omega\frac{K_2}{2}\right]$$

5-3 Type $\mathcal{A}$ VFO operator HOSIDFs

Just like the SIDF, the HOSIDFs are derived for the more general type $\mathcal{A}$ PID switching scheme (Fig. 5-4). For an input $e = Asin(\omega t)$, the real and imaginary parts of the n^{th} order HOSIDF are obtained as :

$$\begin{aligned} Re({}^{\mathcal{A}}H_n^{PID-PID}(A,\omega)) &= \frac{2}{TA}\int_0^T \hat{u}(t)\sin(n\omega t)dt \\ Im({}^{\mathcal{A}}H_n^{PID-PID}(A,\omega)) &= \frac{2}{TA}\int_0^T \hat{u}(t)\cos(n\omega t)dt \end{aligned} \tag{5-6}$$

Solving Equation (5-6) using $\hat{u}$ from Equation (5-4), we get :

$$
\begin{aligned}
{}^{\mathcal{A}}H_n^{PID-PID}(\omega) = &\left[\frac{-2(K_{i1}-K_{i2})\sin\left(n\frac{\pi}{2}\right)}{\pi\omega(n^2-1)}\left(\cos\left(n\pi\right)+n\sin\left(n\frac{\pi}{2}\right)\right)\right.\\
&+4\frac{\left(K_{i1}-K_{i2}\right)}{n\pi\omega}\cos\left(n\frac{\pi}{2}\right)\sin\left(n\frac{3\pi}{4}\right)\sin\left(n\frac{\pi}{4}\right)\\
&\left.+\frac{2\omega(K_{d1}-K_{d2})\sin\left(n\frac{\pi}{2}\right)}{\pi(n^2-1)}\left(\cos\left(n\pi\right)+n\sin\left(n\frac{\pi}{2}\right)\right)\right]\\
&+j\left[\frac{-2(K_{p1}-K_{p2})\sin\left(n\frac{\pi}{2}\right)}{\pi(n^2-1)}\left(n\cos\left(n\pi\right)+\sin\left(n\frac{\pi}{2}\right)\right)\right]
\end{aligned}
\tag{5-7}
$$

Just like the SIDF, the HOSIDFs are also independent of the input amplitude. Note that, $\sin\left(n\frac{\pi}{2}\right)$ is 0 when n is an even integer and $\sin\left(n\frac{\pi}{4}\right)$ is 0 for $n \in \{4, 8, 12, ..\}$. The implication is that for order combinations P-D and D-P, all the even order HOSIDFs are 0, while the ones involving the I operator, only have alternate even order HOSIDFs as 0. Also note that, this analytical equation for the HOSIDFs cannot be used to obtain the SIDF by plugging in $n = 1$ because of the $(n^2 - 1)$ term in the denominator.

5-4 Type $\mathcal{B}$ VFO operator SIDF

Similar to the type $\mathcal{A}$ operator, a general SIDF for the type $\mathcal{B}$ switching scheme that switches between 2 PID controllers as shown in Fig. 5-5 is derived. Over one time period of the input $e = A\sin(\omega t)$, the switching signal $e\dot{e}$ behaves as Equation (5-3). The corresponding output $\hat{u}$ of the switching scheme is obtained as :

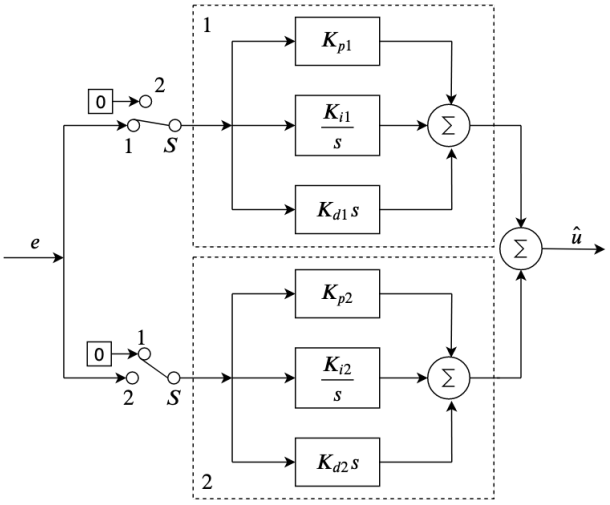

Figure 5-5: Type $\mathcal{B}$ switching scheme, switching between two PID controllers instead of just two FO operators.

$$\hat{u} = \begin{cases} \overbrace{K_{p1}A\sin(\omega t)}^{P} + \overbrace{\frac{1}{\omega}K_{i1}A\big[1-\cos(\omega t)\big]}^{I} + \overbrace{\omega K_{d1}A\cos(\omega t)}^{D} & \text{for } t \in [0, \frac{T}{4}] \\ K_{p2}A\sin(\omega t) + \frac{1}{\omega}A\big[K_{i1} - K_{i2}\cos(\omega t)\big] + \omega K_{d2}A\cos(\omega t) & \text{for } t \in [\frac{T}{4}, \frac{T}{2}] \\ K_{p1}A\sin(\omega t) + \frac{1}{\omega}A\big[-K_{i1}\cos(\omega t) + K_{i2}\big] + \omega K_{d1}A\cos(\omega t) & \text{for } t \in [\frac{T}{2}, \frac{3T}{4}] \\ K_{p2}A\sin(\omega t) + \frac{1}{\omega}K_{i2}A\big[1-\cos(\omega t)\big] + \omega K_{d2}A\cos(\omega t) & \text{for } t \in [\frac{3T}{4}, T] \end{cases} \tag{5-8}$$

The output is same as that of the type $\mathcal{A}$ PID switching scheme in terms of the proportional and derivative parts but differs for integral part. This is because the integrator is a memory element and hence continues to contribute its integrated sum to $\hat{u}$ even when it is receiving 0 input.

In Equation(5-8), a critical assumption has been made for the D part in $\hat{u}$. In type $\mathcal{A}$ switching scheme, the D operators receive a sinusoidal input ($A\sin(\omega t)$) without any discontinuities and hence the derivative is given by $\omega K_d A\cos(\omega t)$. However, as can be seen from Fig. 5-6, the input going into the branches of type $\mathcal{B}$ switching scheme has discontinuities, leading to the theoretical derivative operator to be infinity at those instances and being $\omega K_d A\cos(\omega t)$, immediately at the next instance. Considering the fact that for an actual implementation, the D operator would have an accompanying high frequency pole, and hence have a finite value at the discontinuities, with the transient dying away quickly to give $\omega K_d A\cos(\omega t)$ at steady state, we have approximated the output of the D operator as $\omega K_d A\cos(\omega t)$, neglecting the spikes.

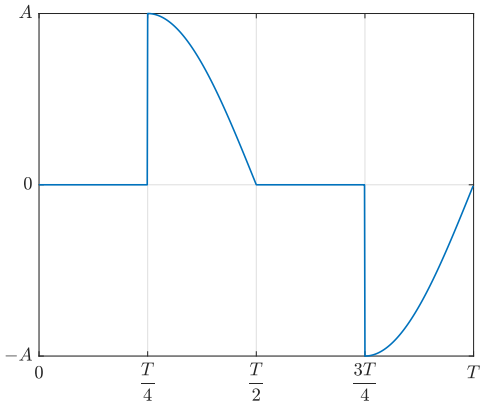

Figure 5-6: For an input $e = A\sin(\frac{2\pi t}{T})$ to the type $\mathcal{B}$ switching scheme, this figure depicts the input received by the operators in branch 2 of the scheme. It can be seen that the signal has discontinuities at $\frac{T}{4}$ and $\frac{3T}{4}$. Similarly, the input to branch 1 also has discontinuities at the same instances.

Solving Equation (5-2) for the $\hat{u}$ from Equation (5-8), we get

$$
\begin{aligned}
{}_{\mathcal{B}}N^{PID-PID}(\omega) = &\left[\left(\frac{K_{p1}+K_{p2}}{2}\right)+\frac{1}{\omega}\left(\frac{K_{i1}-K_{i2}}{\pi}\right)+\omega\left(\frac{K_{d1}-K_{d2}}{\pi}\right)\right] \\
&+j\left[\left(\frac{K_{p1}-K_{p2}}{\pi}\right)+\frac{-1}{\omega}\left(\frac{K_{i1}+K_{i2}}{2}\right)+\omega\left(\frac{K_{d1}+K_{d2}}{2}\right)\right]
\end{aligned} \tag{5-9}
$$

As a consequence of the similarity in the outputs of the two switching schemes, the type $\mathcal{B}$ SIDF is the same as type $\mathcal{A}$ and differs only for the term with integral gains in the real part of the SIDF. Hence, the SIDFs for the P-D and D-P operators for both the switching schemes are the same.

5-5 Type $\mathcal{B}$ VFO operator HOSIDFs

The n^{th} order HOSIDF for the type $\mathcal{B}$ PID-PID switching scheme is obtained by solving Equation (5-6) for the $\hat{u}$ from Equation (5-8).

$$
\begin{aligned}
{}_{\mathcal{B}}H_n^{PID-PID}(\omega) = &\left[\frac{-2(K_{i1}-K_{i2})\sin\left(n\frac{\pi}{2}\right)}{\pi\omega(n^2-1)}\left(\cos\left(n\pi\right)+n\sin\left(n\frac{\pi}{2}\right)\right)\right. \\
&+2\frac{\left(K_{i1}-K_{i2}\right)}{n\pi\omega}\sin^2\left(n\frac{\pi}{2}\right) \\
&\left.+\frac{2\omega(K_{d1}-K_{d2})\sin\left(n\frac{\pi}{2}\right)}{\pi(n^2-1)}\left(\cos\left(n\pi\right)+n\sin\left(n\frac{\pi}{2}\right)\right)\right] \\
&+j\left[\frac{-2(K_{p1}-K_{p2})\sin\left(n\frac{\pi}{2}\right)}{\pi(n^2-1)}\left(n\cos\left(n\pi\right)+\sin\left(n\frac{\pi}{2}\right)\right)\right]
\end{aligned} \tag{5-10}
$$

As all the terms in Equation (5-10) have $\sin\left(n\frac{\pi}{2}\right)$, the even order HOSIDFs are 0 for all 6 type $\mathcal{B}$ VFO operators.

5-6 VFO operator selection

Next step is to analyse the SIDFs of the VFO operators and short-list the order combinations which are useful from a control perspective. Since the goal is to build a VFO controller in the PID-loop shaping framework, the short-listing is done by comparing the SIDF based frequency response of the VFO operators with the frequency response of the corresponding linear filters in a PID controller. Here a series form of PID controller [40] is considered and given as :

$$
C^{PID} = K\underbrace{\left(1+\frac{\omega_i}{s}\right)}_{\text{P-I}}\underbrace{\left(\frac{s}{w_d}+1\right)}_{\text{P-D}}\frac{1}{\left(\frac{s}{w_t}+1\right)}\frac{1}{\left(\frac{s}{\omega_f}+1\right)} \tag{5-11}
$$

where K is the overall gain, ω_i is the corner frequency of the P-I filter where the integrator action rolls off, ω_d is the corner frequency in the theoretical P-D filter where the derivative action starts and ω_t is its taming frequency and ω_f is the frequency of the loss pass filter[2]. The P-I part is employed to increase controller gain at frequencies below the closed loop bandwidth but the integrator brings in a 90° phase lag which requires ω_i to be placed at least a decade before the bandwidth to allow the phase to recover. The P-D part along with the $1/\left(\frac{s}{w_t}+1\right)$, i.e., band limited derivative action is employed in the frequency range $[\omega_d,\omega_t]$ to achieve the desired phase at the bandwidth. In the following subsections, the VFO operators will be analysed to see if they have more advantageous frequency responses as compared to their linear counterparts.

5-6-1 Type $\mathcal{A}$ and $\mathcal{B}$ P-I and I-P operators

These operators are compared with a linear P-I filter, with $\omega_i = 2\pi$ rad/s. The gains K_1 and K_2 of the VFO operators are tuned so that their frequency response magnitude matches that of the linear P-I filter. To illustrate how the gains affect the frequency response of the operators, 3 sets of gains for an $\mathcal{A}$ P-I operator, as given in Table 5-1, are considered and the corresponding frequency responses are shown in Fig. 5-7. From cases 1 and 2, it can be seen that, by adjusting the ratio of K_1 and K_2 the corner frequency can be moved. Then in case 3, the ratio is kept same as in case 2, while increasing both gains by the same factor, and it can be seen that the overall magnitude of the frequency response can be adjusted while keeping the same corner frequency. This method of tuning the gains is applicable for the other operators as well.

	K_1	K_2
Case 1	1	1
Case 2	1	2π
Case 3	10	20π

Table 5-1: Three sets of gains for a type $\mathcal{A}$ P-I operator to illustrate their effect on its frequency response as shown in Fig. 5-7.

The tuned gains for $\mathcal{A}$ and $\mathcal{B}$ P-I and I-P operators are presented in Table 5-2 and the corresponding frequency responses of the VFO operators and the linear P-I filter are shown in Fig. 5-8.

	K_1	K_2
$\mathcal{A}$ P-I	1.687	10.6
$\mathcal{A}$ I-P	10.6	1.687
$\mathcal{B}$ P-I	1.687	10.6
$\mathcal{B}$ I-P	10.6	1.687

Table 5-2: Gains of Type $\mathcal{A}$ and $\mathcal{B}$ P-I and I-P operators to have the same frequency response magnitude as a linear P-I filter with $\omega_i = 2\pi$ rad/s.

The frequency response magnitude of $\mathcal{A}$ P-I and I-P operators exactly matches that of the linear P-I filter at all frequencies, while that of $\mathcal{B}$ P-I and I-P operators matches the linear P-I

[2]Refer appendix A for a brief account on loop shaping terminology.

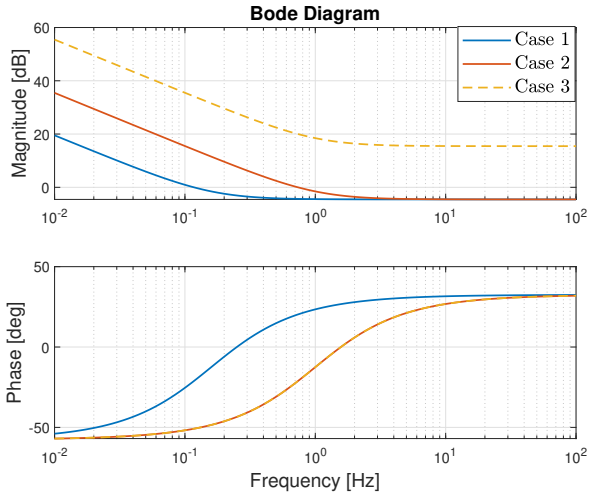

Figure 5-7: Frequency response of the type $\mathcal{A}$ P-I operator for three different cases of gains K_1, K_2 given in Table 5-1.

except in $[\frac{\omega_i}{10}, 10\omega_i]$. Considering the phase, it can be seen that $\mathcal{A}$ P-I provides a phase lead of 32.5° at all frequencies as compared to the linear filter. This phase advantage, especially above $10\omega_i$ can prove to be beneficial, since if $\mathcal{A}$ P-I operator were to replace a linear P-I filter in the PID controller, then the linear P-D filter will have to provide lesser phase lead at the bandwidth to get the same phase margin. Similar phase advantage is seen for $\mathcal{B}$ P-I, which even though starts off at −122.5° at low frequencies, rises quickly within 2 decades around ω_i to provide a phase of 32.5°, beyond $10\omega_i$. Due to the steep rise in phase, not only is it able to give a slightly higher phase lead as compared to $\mathcal{A}$ P-I in a brief frequency range from $[2\omega_i, 10\omega_i]$ but due to its flatness of phase in that region, it can potentially also provide robustness against plant gain variations. Meanwhile, both $\mathcal{A}$ I-P and $\mathcal{B}$ I-P have a phase lag as compared to the linear P-I at frequencies above $10\omega_i$ and hence do not appear advantageous.

5-6-2 Type $\mathcal{A}$ and type $\mathcal{B}$ P-D and D-P operators

Similar to the P-I case, the gains of these VFO operators are tuned so as to match the frequency response magnitude with that of a linear theoretical P-D filter (i.e., without a taming pole) with $\omega_d = 2\pi$ rad/s. The tuned gains are presented in Table 5-3 and the corresponding frequency responses of the VFO operators and the linear P-D filter are shown in Fig. 5-9.

	K_1	K_2
$\mathcal{A}$ P-D	1.687	0.269
$\mathcal{A}$ D-P	0.269	1.687
$\mathcal{B}$ P-D	1.687	0.269
$\mathcal{B}$ D-P	0.269	1.687

Table 5-3: Gains of type $\mathcal{A}$ and $\mathcal{B}$ P-D and D-P operators to have the same frequency response magnitude as a theoretical linear P-D filter with $\omega_d = 2\pi$ rad/s.

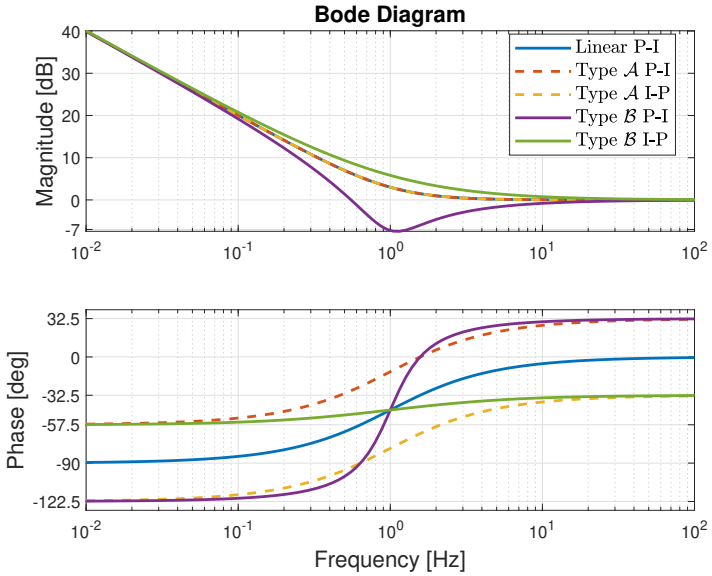

Figure 5-8: Frequency Responses of Linear P-I filter and Type $\mathcal{A}$ and Type $\mathcal{B}$ P-I and I-P VFO operators.

As pointed out previously, it can be seen from Fig. 5-9 that the frequency responses for type $\mathcal{A}$ P-D and D-P operators are same as $\mathcal{B}$ P-D and D-P operators respectively since their SIDFs are the same. Both P-D operators provide phase lead of 32.5° as compared to the linear P-D at all frequencies. In the PID controller, wider the $[\omega_d,\omega_t]$ band to achieve the desired phase margin, higher becomes the controller gain at higher frequencies (deteriorated noise attenuation) and lower at lower frequencies (deteriorated reference tracking.) If a type $\mathcal{A}$ or $\mathcal{B}$ P-D operator were to replace the P-D part in the PID controller, then owing to their phase lead, the $[\omega_d,\omega_t]$ band can be narrower and hence prove advantageous. $\mathcal{A}$ and $\mathcal{B}$ D-P operators don't seem lucrative due to their phase lag of 32.5° at all frequencies as compared to linear P-D.

5-6-3 Type $\mathcal{A}$ and $\mathcal{B}$ D-I and I-D operators

The gains of these VFO operators are tuned so as to match their frequency response magnitude with that of a linear theoretical I-D filter given as:

$$C^{I-D} = \left(1 + \frac{\omega_d}{s}\right)\left(\frac{s}{\omega_d} + 1\right)$$

For $\omega_d = 2\pi$ rad/s, the tuned gains are presented in Table 5-4 and the corresponding frequency responses of the VFO operators and the linear I-D filter are shown in Fig. 5-10.

Outside the $[0.2\omega_d,5\omega_d]$ frequency range, the magnitudes of all the 4 operators exactly match that of the linear I-D filter. In that range, type $\mathcal{A}$ operators' magnitude still remains close to that of the linear filter but that of the type $\mathcal{B}$ operators deviates quite a lot and goes to 0 at ω_d. If a VFO I-D or D-I operator were to replace this linear I-D filter, then it would prove advantageous if it had higher phase after ω_d than the linear filter. The only operator

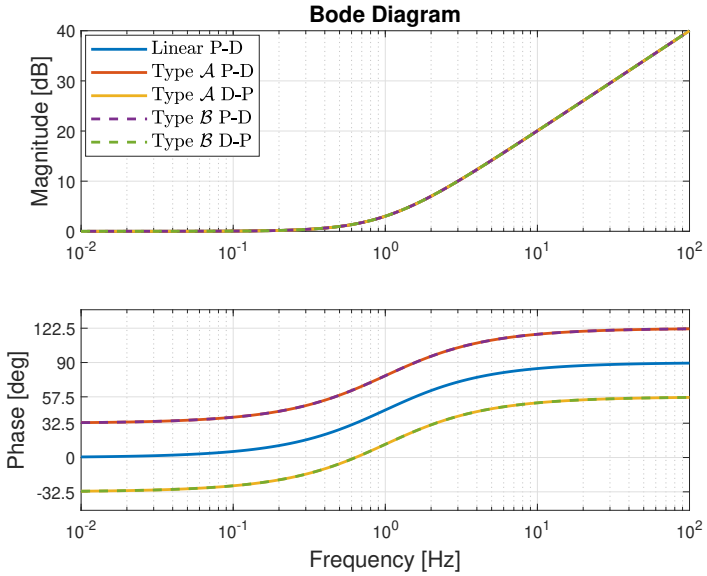

Figure 5-9: Frequency Responses of Linear P-D filter and type $\mathcal{A}$ and type $\mathcal{B}$ P-D and D-P VFO operators.

	K_1	K_2
$\mathcal{A}$ I-D	10.6	0.269
$\mathcal{A}$ D-I	0.269	10.6
$\mathcal{B}$ I-D	10.6	0.269
$\mathcal{B}$ D-I	0.269	10.6

Table 5-4: Gains of type $\mathcal{A}$ and $\mathcal{B}$ P-D and D-P operators to have the same frequency response magnitude as a theoretical linear P-D filter with $\omega_d = 2\pi\,\mathrm{rad/s}$.

that appears advantageous in this sense is the $\mathcal{B}$ I-D operator, but its magnitude is quite low around ω_d. Moreover, since an I-D filter is not commonly used in the PID control framework, the D-I and I-D operators are being left out of the scope of this research.

This selection process has resulted in the selection of $\mathcal{A}$ P-I (${}^{\mathcal{A}}\mathscr{D}^{P-I}$), $\mathcal{B}$ P-I (${}^{\mathcal{B}}\mathscr{D}^{P-I}$), $\mathcal{A}$ P-D (${}^{\mathcal{A}}\mathscr{D}^{P-D}$) and $\mathcal{B}$ P-D (${}^{\mathcal{B}}\mathscr{D}^{P-D}$) VFO operators for building the VFO controllers.

5-7 VFO controller tuning

Now, the method to tune the VFO controllers is presented. The process is two-fold, firstly constituting of tuning the gains K_1 and K_2 of the VFO operators and secondly choosing the corresponding linear filter and tuning its parameters. The VFO controllers are built by replacing the linear filters in the PID controller (Equation (5-11)) with the corresponding VFO operators. The VFO controller using $\mathcal{A}$ or $\mathcal{B}$ P-I operators is shown in Fig. 5-11 and using P-D operators is shown in Fig. 5-12.

As the aim is to implement the controllers for a precision positioning stage, which can be modelled as a mass-spring damper system, the tuning guidelines are presented for controlling

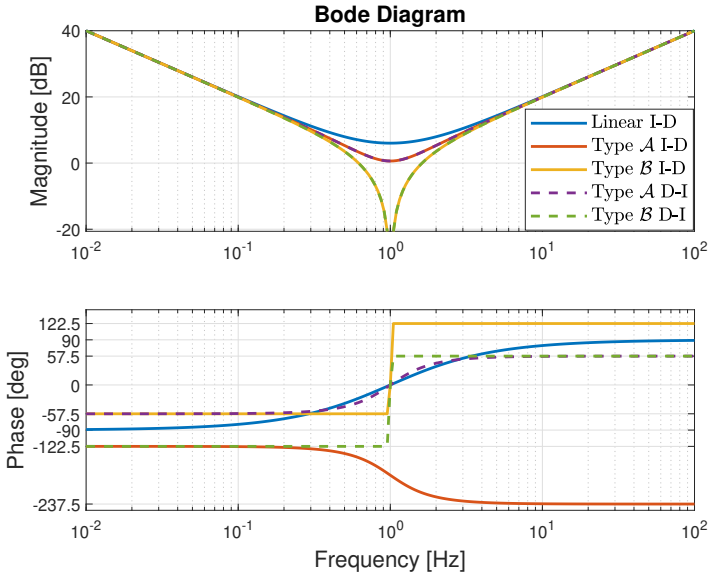

Figure 5-10: Frequency Responses of Linear I-D filter and type $\mathcal{A}$ and type $\mathcal{B}$ I-D and D-I VFO operators.

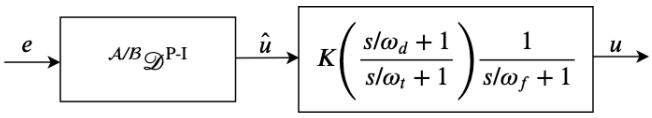

Figure 5-11: Block diagram of a VFO controller using type $\mathcal{A}$ P-I or type $\mathcal{B}$ P-I operator denoted as ${}^{\mathcal{A}}C^{P-I}$ or ${}^{\mathcal{B}}C^{P-I}$ respectively.

such a system with the bandwidth beyond the resonance frequency where the system phase is $-180°$. For such an application, the PID controller with a rule of thumb set of parameters [40] gives a phase margin of 42°. For fair comparison of the closed loop performance of the VFO controllers and this rule of thumb PID controller, the VFO controllers are tuned for the same bandwidth and phase margin as this PID controller.

5-7-1 Rule of thumb PID controller

For controlling a plant G for a bandwidth of ω_c rad/s , as a rule of thumb, the PID controller parameters are given as [40][3] :

$$\omega_i = \frac{\omega_c}{10},\ \omega_d = \frac{\omega_c}{3},\ \omega_t = 3\omega_c,\ \omega_f = 10\omega_c$$

and the gain K is given by

$$K = \frac{1}{3|G(j\omega_c)|}$$

where $|G(j\omega_c)|$ is the magnitude of plant gain at ω_c.

[3] A brief on rule of thumb PID controller can be found in Appendix section A-2.

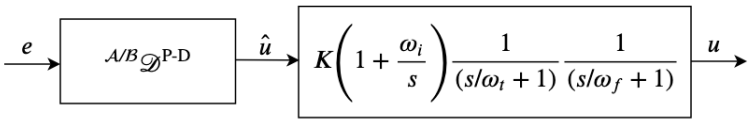

Figure 5-12: Block diagram of a VFO controller using type $\mathcal{A}$ P-D or type $\mathcal{B}$ P-D operator denoted as ${}^{\mathcal{A}}C^{P-D}$ or ${}^{\mathcal{B}}C^{P-D}$ respectively.

5-7-2 VFO controllers using type $\mathcal{A}$ P-I operator (${}^{\mathcal{A}}C^{P-I}$) and type $\mathcal{B}$ P-I operator (${}^{\mathcal{B}}C^{P-I}$)

For these controllers, the frequency response to be shaped is given by :

$$ {}^{\mathcal{A}/\mathcal{B}}C^{P-I}(\omega) = K\left({}^{\mathcal{A}/\mathcal{B}}N^{P-I}(\omega)\right)\left(\frac{j\omega}{w_d}+1\right)\frac{1}{\left(\frac{j\omega}{w_t}+1\right)}\frac{1}{\left(\frac{j\omega}{\omega_f}+1\right)} \tag{5-12}$$

- The gains K_1 and K_2 of the VFO P-I operators are tuned such that the corner frequency in their frequency response is same as that in a linear P-I filter. This is done by setting

$$K_1 = 1 \quad K_2 = \omega_i = \frac{\omega_c}{10}$$

- The low pass filter (LPF) has the corner frequency at $\omega_f = 10\omega_c$, same as that for the linear PID case. Note that this brings in a phase lag of 5° at ω_c.
- Next, the $[\omega_d,\omega_t]$ band of the linear band limited derivative action is tuned. In the linear PID controller, a band of $[\frac{\omega_c}{3},3\omega_c]$ provides a phase margin of 42°. But since the VFO P-I operators with gains tuned in the previous step, provide a phase of about 32° at ω_c, the derivative action has to provide less phase and $[\omega_d,\omega_t]$ band can be narrower. The band is parametrized as $[\frac{\omega_c}{a},a\omega_c]$ and solved for a to get the phase of 42° at ω_c.
- Finally the bandwidth is set by the adjusting the overall gain K so that the frequency response gain magnitude of these VFO controllers at ω_c becomes equal to $1/|G(j\omega_c)|$.
- While deriving the describing functions, it is assumed that the $\dot{e}$ required for the switching signal is computed using an ideal derivative operator, i.e. having a phase lead of 90° at all frequencies. However for practical implementation, the derivative filter is made proper with a pole at $10\omega_c$. Placing the pole at a frequency lower than this, would start bringing in the phase lag even before ω_c, and thereby changing the switching instances for the frequencies of interest, as compared to the instances in the case of an ideal derivative operator. Placing it at $10\omega_c$ just brings in a phase lag of 5° at ω_c. Also, it is not placed any higher so as to bring in the low pass filtering as soon as possible.

5-7-3 VFO controllers using type $\mathcal{A}$ P-D operator (${}^{\mathcal{A}}C^{P-D}$) and type $\mathcal{B}$ P-D operator (${}^{\mathcal{B}}C^{P-D}$)

For these controllers, the frequency response to be shaped is given by :

$$ {}^{\mathcal{A}/\mathcal{B}}C^{P-D}(\omega) = K\left(1+\frac{\omega_i}{j\omega}\right)\left({}^{\mathcal{A}/\mathcal{B}}N^{P-D}(\omega)\right)\frac{1}{\left(\frac{j\omega}{w_t}+1\right)}\frac{1}{\left(\frac{j\omega}{\omega_f}+1\right)} \tag{5-13}$$

- The linear P-I part in these VFO controllers has the same corner frequency as the P-I filter in the PID controller, i.e., at $\omega_i = \frac{\omega_c}{10}$ thereby allowing the phase to recover from 90° phase lag to just 5° phase lag at ω_c.
- The low pass filter (LPF) has the corner frequency at $\omega_f = 10\omega_c$, same as that for the linear PID case which brings in a phase lag of 5° at ω_c.
- Next, the gains K_1 and K_2, and ω_t are iteratively tuned by parametrizing them in terms of 'a' such that :

  $$K_1 = \frac{\omega_c}{a} \quad K_2 = 1 \quad \omega_t = a\omega_c$$

  Starting from $a = 3$, reduce a till the obtained phase at ω_c is 42°.
- Finally the bandwidth is set by the adjusting the overall gain K so that the frequency response gain magnitude of these VFO controllers at ω_c becomes equal to $1/|G(j\omega_c)|$.
- For practical implementation, the D operator in the VFO operator is made proper with a high frequency pole at $100\omega_c$.
- Again the derivative operator required to compute $\dot{e}$ for the switching signal has an accompanying pole at $10\omega_c$, just like in the P-I case.

A plot comparing the controller frequency response of a linear PID controller with that of the VFO controllers is presented in Fig. 5-13.

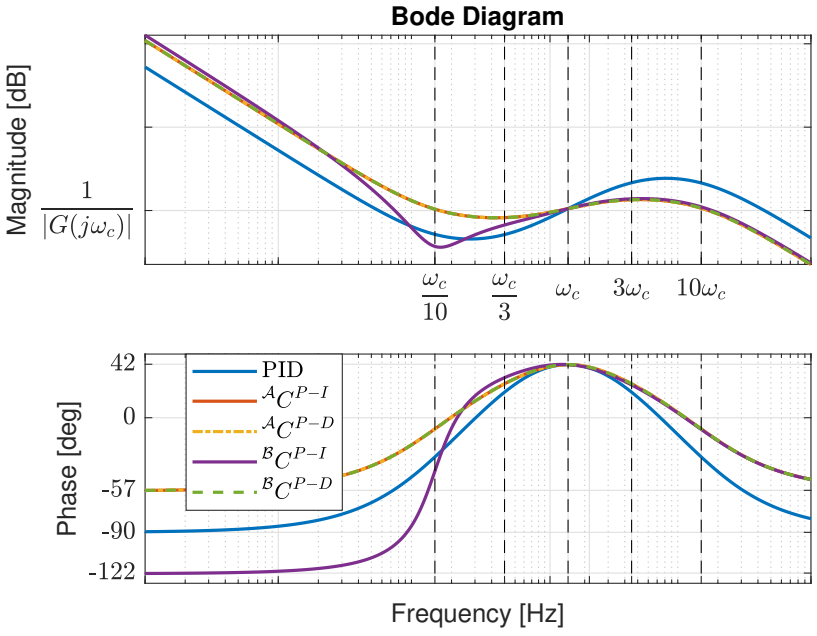

Figure 5-13: Frequency response of linear PID and the VFO controllers, where ω_c is the desired closed loop bandwidth and $|G(j\omega_c)|$ is the magnitude of the plant gain ω_c.

As can be seen from Fig. 5-13, all controllers have a magnitude of $1/|G(j\omega_c)|$ at ω_c and hence in combination with the plant, will be able to achieve the open loop crossover frequency at ω_c.

Also, all the controllers have a phase of 42° at ω_c, thereby meeting phase margin requirement. Since all the VFO controllers have gain higher than that of PID below ω_c and lower than that of PID above ω_c, these controllers can potentially outperform linear PID in reference tracking, disturbance rejection and noise attenuation. The closed loop performance of these controllers shall be analysed in the next chapter by performing experiments on a precision positioning stage.

Chapter 6

Experimental Results

Tuning the 4 VFO controllers using the guidelines from the previous chapter, their closed loop performance in controlling a precision positioning stage is now analysed. Firstly, the setup used for the experiments is described and the corresponding model is identified. This is followed by presenting and discussing the experimental results.

6-1 Experiment setup and identification

The experiments are carried out on a planar, 3 DOF precision positioning 'Spider' stage as shown in Fig. 6-1. The system consists of 3 identical masses (M), individually actuated by dedicated voice coil actuators (C). The masses are attached to the base plate by means of leaf flexures (F) which provide stiffness. Mercury M2000 linear encoders (E) positioned below the masses, measure their position with a resolution of 100 nm. These individual masses are attached to the central stage 'S' by means of leaf flexures, thus making it a MIMO system. However for the experiments, only the sub-assembly 1 (highlighted in green) is controlled, thus reducing it to a SISO system. The controllers are programmed in Labview and implemented on the National Instruments cRIO FPGA for deterministic real time control. The analog output module NI 9264 is used to send the generated control signal to the linear power amplifier which actuates the voice coil. The linear encoder is read via the NI 9401 digital input/output module.

The actuator has a software implemented saturation of 30000 counts to prevent damage to the setup. To avoid introducing this saturation non-linearity, experiments are performed by adjusting the input signal amplitudes such that the actuator saturation is not hit. A possible source of implementation artefacts in the experiments is quantization. The input signal generated by the controller is typecast to a 16 bit integer, owing to the 16 bit resolution of the NI 9264 module. The setup is placed on a vibration isolation table. In the unactuated state, the encoder measurement fluctuates between ±3 counts (i.e., ±300nm).

The overall plant G, comprising of the NI 9264 module, amplifier, actuator, actuated sub-assembly 1, encoder and NI 9401 module, is identified. The input to this plant is applied in

integer counts (1 count = 0.3mV) and the output is also measured in integer counts (1 count = 100nm). The frequency response of the plant, measured from 0.1Hz to 500Hz using a chirp signal is shown in Fig. 6-2. The fourth order model identified using this FRF data is also plotted in the same figure and presented in Equation (6-1). The identified model is similar to a collocated double mass-spring-damper system.

$$G(s) = \frac{8.37e3s^2 + 1.63e4s + 5.92e7}{s^4 + 4.64s^3 + 1.44e4s^2 + 3.31e4s + 5.14e7} \tag{6-1}$$

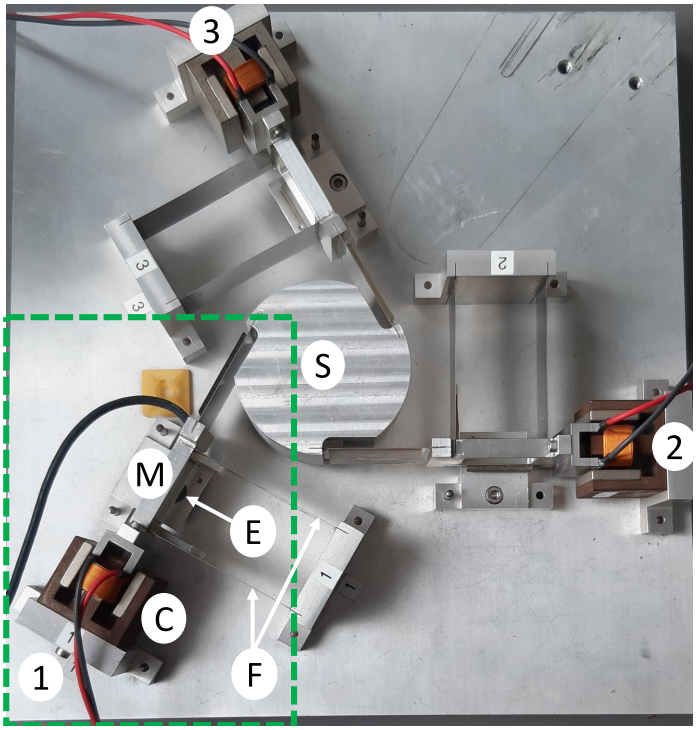

Figure 6-1: Planar, 3 DOF precision positioning 'Spider' Stage, of which only sub-assembly 1 (highlighted in green) is used for the experiments. S is the central stage, M is the actuated mass, C is the voice coil actuator, E is the linear encoder and F are leaf flexures.

For this plant, the PID and VFO PID controllers are tuned as per the guidelines in Section 5-7 for a bandwidth of $\omega_c = 2\pi\,150\,\text{rad/s}$. The tuned parameter values are presented in Table 6-1. The operators within the VFO operators and the corresponding linear filters are all discretized for a sampling frequency of 10 KHz using Tustin's method. The closed loop, as depicted in Fig. B-1 has 3 exogenous inputs, namely the tracking reference r, input disturbance d_u and measurement noise n_m, the performance of the closed loop to which will be analysed in reference tracking, disturbance rejection and noise attenuation experiments respectively. Additionally the step response characteristics are also examined.

Numerical simulations are performed to determine the closed loop stability of the VFO controllers, as a mathematical proof could not be derived. Experiments are performed for ${}^{\mathcal{A}}C^{P-I}$, ${}^{\mathcal{B}}C^{P-I}$ and ${}^{\mathcal{A}}C^{P-D}$ controllers as steady state was reached in their simulations, but ${}^{\mathcal{B}}C^{P-D}$ simulations showed instability and hence is not considered for the experiments. A possible

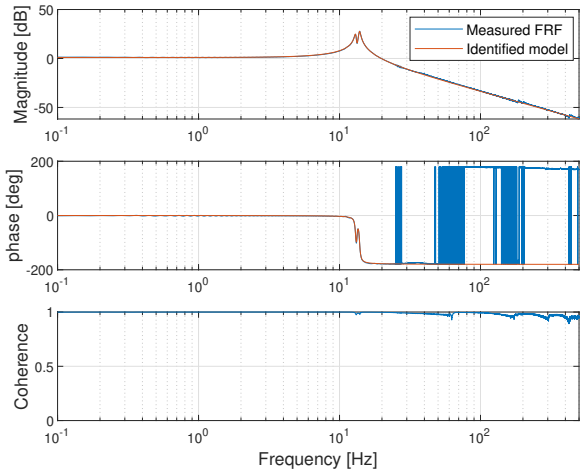

Figure 6-2: Measured frequency response of the plant G from 0.1Hz to 500Hz and the frequency response of the identified fourth order model.

	K	a
${}^{\mathcal{A}}C^{P-I}$	122.8558	1.4455
${}^{\mathcal{B}}C^{P-I}$	143.4747	1.3664
${}^{\mathcal{A}}C^{P-D}$	0.1884	1.4455
${}^{\mathcal{B}}C^{P-D}$	0.1884	1.4455

Table 6-1: Tuned parameters of the VFO controllers. (Other parameter values are not presented since they can be obtained using a and ω_c.)

cause for the instability of ${}^{\mathcal{B}}C^{P-D}$ is the transient spikes introduced in its output by its derivative operator (D) at every switching instance.

6-2 Higher order open loop frequency responses

The VFO controllers have been tuned to get the desired open loop shape by treating the SIDF based frequency response of the VFO operators as their true frequency response, neglecting the HOSIDF information. From the open loop frequency responses, shown in Fig. 6-4, it can be seen that, as compared to the magnitude of the open loop for the PID controller, the magnitude of the open loop for VFO controllers is higher before the bandwidth and lower beyond the bandwidth. In the linear loop shaping framework, this loop shape for the VFO controllers would translate to better reference tracking, disturbance rejection and noise attenuation characteristics than PID.

The primary assumption in using only the VFO operator SIDF for loop shaping is that the first harmonic content in the VFO operator output is dominant as compared to the higher harmonic content. Although it seems trivial that these higher harmonics will affect the closed loop performance, no concrete method to predict the extent of their effect or incorporate higher order information in controller tuning could be found in literature. In the field of reset control, where a similar SIDF based loop shaping method is used for developing controllers

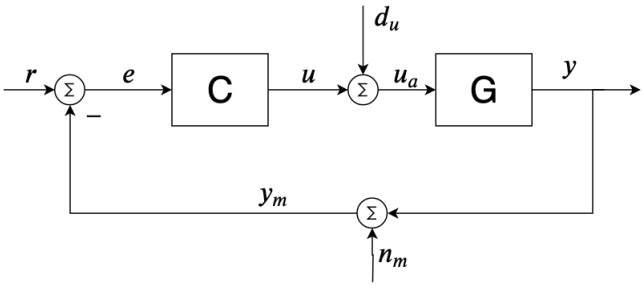

Figure 6-3: Feedback control loop, where C is the controller, G is the plant, r is the tracking reference, d_u is the input disturbance, n_m is the measurement noise, e is the tracking error, u is the generated control input, u_a is the actual input going to the plant and y is the plant output.

using the reset elements, attempts have been made to incorporate the HOSIDF information in controller design [37,38]. These works have looked at the higher order open loop frequency responses to observe relations to the closed loop performance and in this thesis, the same will be done for the VFO controllers.

Considering the open loop in the HOSIDF framework (Section 3-3), a sinusoidal input $A\sin(\omega t)$ entering the VFO operator, is approximated as passing through a virtual harmonics generator which generates higher harmonic signals having the same amplitude A. The generated n^{th} harmonic signal gets a gain and phase as per the n^{th} order HOSIDF ($H_n(\omega)$) of the VFO operator, with the 1^{st} harmonic getting them as per the SIDF ($N(\omega)$). The base frequency signal along with these higher harmonics then pass ahead through the linear filter (LF) and the plant (G) and further get a gain and phase depending on their frequency. The open loop output y is the sum of all these signals and can be formally stated as in Equation (6-2).

$$\begin{aligned} y = &\underbrace{\left|\left(G(j\omega)LF(j\omega)N(\omega)\right)\right|}_{|(\text{open loop})|} A\sin\Big(\omega t + \underbrace{\angle\left(G(j\omega)LF(j\omega)N(\omega)\right)}_{\angle(\text{open loop})}\Big) \\ &+ \sum_{n=2}^{\infty} \underbrace{\left|\left(G(jn\omega)LF(jn\omega)H_n(\omega)\right)\right|}_{|(n^{th}\text{ higher order open loop})|} A\sin\Big(n\omega t + \underbrace{\angle\left(G(jn\omega)LF(jn\omega)H_n(\omega)\right)}_{\angle(n^{th}\text{ higher order open loop})}\Big) \end{aligned} \tag{6-2}$$

The open loop and the higher order open loop frequency responses for the ${}^{\mathcal{A}}C^{P-I}$, ${}^{\mathcal{B}}C^{P-I}$ and ${}^{\mathcal{A}}C^{P-D}$ controllers are presented in Fig. 6-5, 6-6 and 6-7 respectively. While reading these plots, it is important to understand that although Equation (6-2) shows that the n^{th} higher order open loop gives the gain and phase for the signal with frequency $n\omega$, it is actually plotted for the input base frequency ω that caused the generation of $n\omega$.

For all the 3 controllers, the n^{th} higher order open loop shows the resonance peak at a frequency f_r/n where $f_r \approx 14$Hz is the resonance frequency of the plant. Lower the magnitude of the higher order open loop frequency response at a frequency, lower is the magnitude of the higher harmonic content in the open loop output. From Fig. 6-5, it can be seen that for ${}^{\mathcal{A}}C^{P-I}$ controller, the 2^{nd} order open loop actually has slightly higher gain than the open loop until about 9Hz, beyond which the base frequency component will be dominant in the

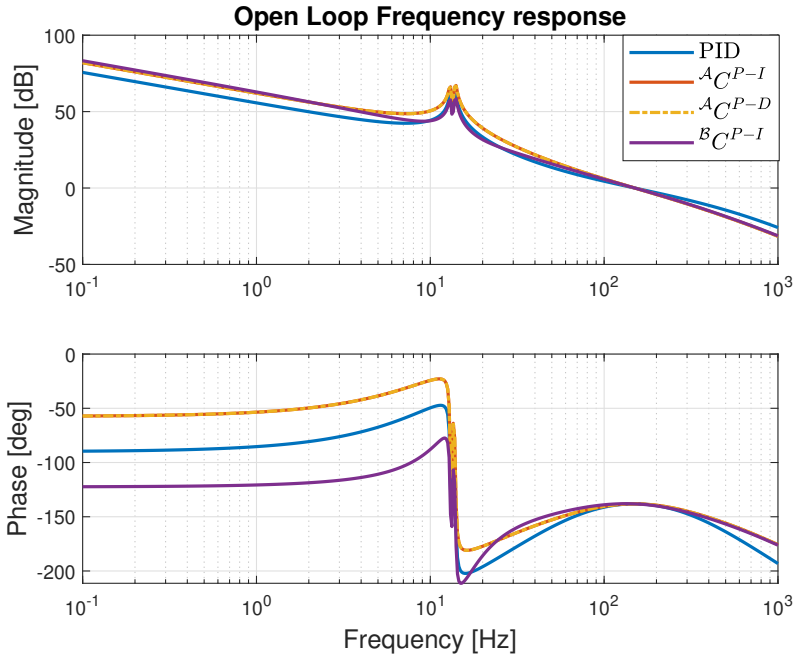

Figure 6-4: Open loop frequency response for the linear PID and VFO controllers.

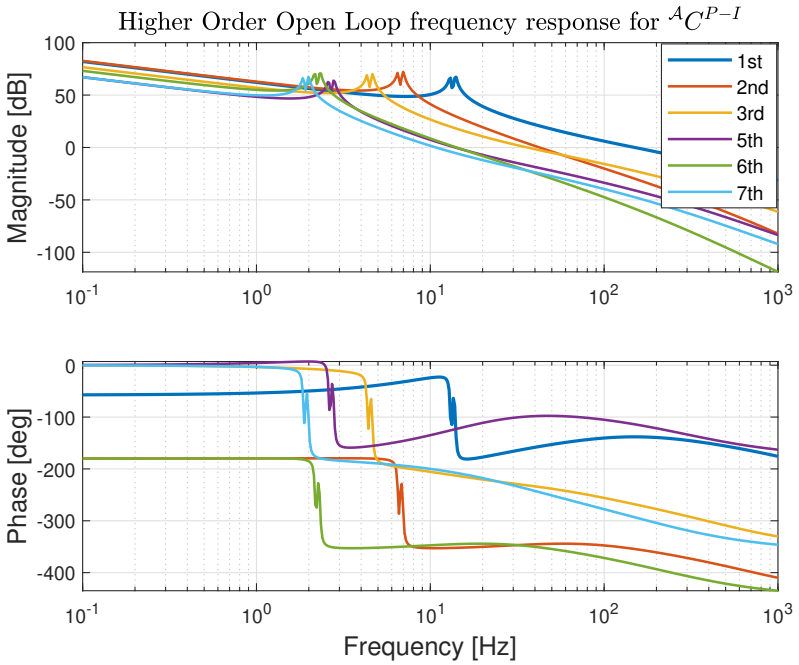

Figure 6-5: Open loop and higher order open loop frequency responses for $^{\mathcal{A}}C^{P-I}$ controller for orders 1 to 7, where 1st denotes the open loop. 4^{th} order is not presented since it is 0, as the alternate even order HOSIDFs for the $\mathcal{A}$ P-I operator are 0.

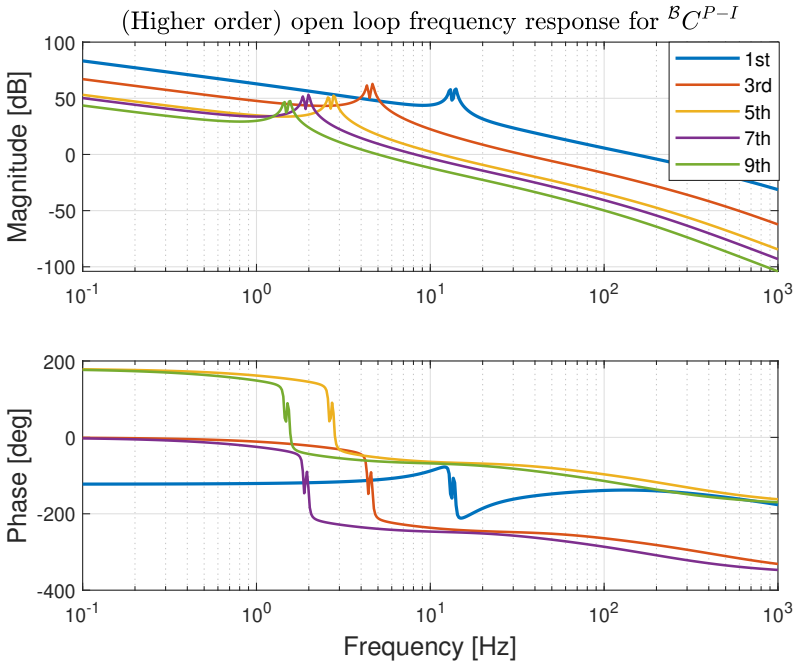

Figure 6-6: Open loop and higher order open loop frequency responses for ${}^{\mathcal{B}}C^{P-I}$ controller for orders 1 to 9, where 1st denotes the open loop. Even orders are not presented since they are 0, as the even order HOSIDFs for the $\mathcal{B}$ P-I operator are 0.

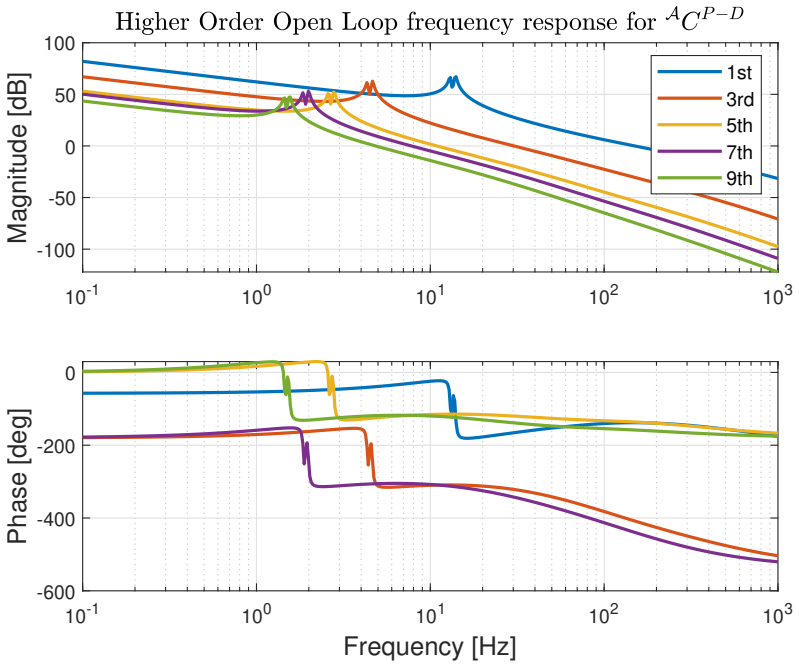

Figure 6-7: Open loop and higher order open loop for ${}^{\mathcal{A}}C^{P-D}$ controller showing the higher order open loop frequency response for orders 1 to 7. All the even order HOSIDFS for the $\mathcal{A}$ P-D operator are 0.

open loop output. For ${}^{\mathcal{B}}C^{P-I}$ and ${}^{\mathcal{A}}C^{P-D}$ controllers, the higher order open loop frequency responses have less magnitude than that of the open loop except for the resonance peaks which come close to open loop magnitude, with the peak of the 3^{rd} order even exceeding the open loop magnitude at that frequency. For these 2 controllers, if the plant is a critically damped or overdamped mass-spring-damper system, then there would not be peaks in the higher order open loop frequency responses and hence there would be no frequency range for which the higher order harmonics are greater in magnitude than the first harmonic in the open loop output.

The purpose of performing the experiments is two-fold. Firstly to verify if the VFO controllers offer better reference tracking, disturbance rejection and noise attenuation as compared to the PID controller, that the open loop shape suggests. Secondly connections between the higher order open loop frequency responses and the closed loop performance are to be drawn by observing the results. Certainly, these objectives can be fulfilled using simulation results alone, but experimental results will additionally serve as a proof of concept for sparking interest in industry. Simulations have been performed to validate the experimental results, and having done so, only the experimental results are discussed in this chapter.

6-3 Noise attenuation

Before checking the control performance to injected artificial noise, the performance for $r = n_m = d_u = 0$ and only the presence of inherent measurement noise in the system (±3 counts) is looked into. $\|\|_\infty$ and $\|\|_2$ norms are taken once steady state has been reached in the experiment. The corresponding values are shown in Table 6-2. For having the same number of samples for the $\|\|_2$ norm, this experiment is carried out for the same duration for all the controllers.

	$\|e\|_\infty$	$\|e\|_2$	$\|u\|_\infty$	$\|u\|_2$
PID	1	20.9	201	3.14e3
${}^{\mathcal{A}}C^{P-I}$	1	61	243	10.47e3
${}^{\mathcal{B}}C^{P-I}$	1	54.8	247	9.8e3
${}^{\mathcal{A}}C^{P-D}$	22	701.1	2225	68.68e3

Table 6-2: Performance of the controllers in the presence of only inherent system noise of ±3 counts and $r = n_m = d_u = 0$. 1 count of e is 100nm and 1 count of u is 0.3mV.

Both ${}^{\mathcal{A}}C^{P-I}$ and ${}^{\mathcal{B}}C^{P-I}$ controllers are able to maintain the tracking error within ±1 count like the PID controller. However, it must be noted from $\|e\|_2$ norm, that the PID controller is able to keep e at 0 for more samples than these 2 controllers. Similarly, even though the max control input is comparable to that of PID, the $\|u\|_2$ norm reflects the higher demand for control action over the course of the experiment. The ${}^{\mathcal{A}}C^{P-D}$ controller struggles to keep the output at 0, with error going as high as 22 counts, while also commanding very high control inputs.

Now white measurement noise with different amplitudes ranging from 5 to 50 counts is applied and the corresponding values of $\|e\|_\infty$ are presented in Table 6-3. It can be seen that, despite lower open loop gain as compared to PID beyond the bandwidth, the VFO controllers are

	$\|n_m\|_\infty = 5$	$\|n_m\|_\infty = 10$	$\|n_m\|_\infty = 30$	$\|n_m\|_\infty = 50$
PID	3	7	23	34
${}^{\mathcal{A}}C^{P-I}$	6	14	43	54
${}^{\mathcal{B}}C^{P-I}$	8	15	45	72
${}^{\mathcal{A}}C^{P-D}$	258	-	-	-

Table 6-3: $\|e\|_\infty$ (1 count = 100nm) for the different controllers in the presence of white measurement noise n_m of different amplitudes.

	T_r(sec)	T_s(sec)	Overshoot (%)	$\|u\|_\infty$
PID	9.7321e-4	192e-4	43	19.7e3
${}^{\mathcal{A}}C^{P-I}$	12e-4	570e-4	50	20.9e3
${}^{\mathcal{B}}C^{P-I}$	11e-4	166e-4	52	22.2e3
${}^{\mathcal{A}}C^{P-D}$	88e-4	-	-	5.1e3

Table 6-4: Step response characteristics for a reference step of 100 counts (10 µm), and 1 count of the control input is 0.3mV.

unable to attenuate noise, especially with ${}^{\mathcal{A}}C^{P-D}$ controller drastically amplifying it. Experiments for noise amplitudes higher than 5 counts, could not be carried out for ${}^{\mathcal{A}}C^{P-D}$ since actuator saturation is hit.

6-4 Step response

For a reference step of amplitude 100 counts (10 µm), Fig. 6-8 shows the closed loop step response for different controllers and Table 6-4 shows the corresponding performance metrics. Rise time (T_r) is the time taken for the output to go from 10 percent to 90 percent of its steady state value and the settling time (T_s) is the time taken by the output to reach and stay within 2 percent of steady state value.

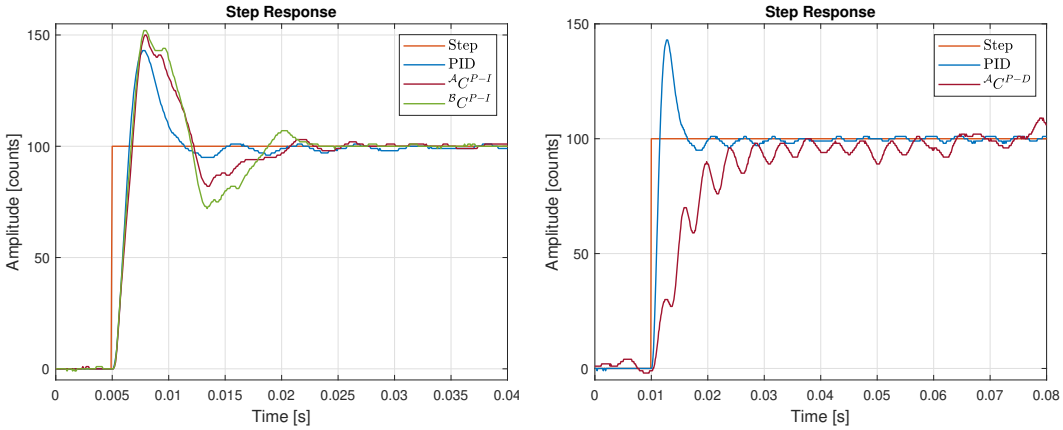

Figure 6-8: Step responses of the VFO controllers for a reference step of 100 counts (10 µm).

Despite having the same phase margin as the linear PID controller, ${}^{\mathcal{A}}C^{P-I}$ and ${}^{\mathcal{B}}C^{P-I}$ controllers have greater overshoots and the output for ${}^{\mathcal{A}}C^{P-I}$ even settles slowly than that for

PID. But on the bright side, the settling time for ${}^{\mathcal{B}}C^{P-I}$ is lower than that for PID. For ${}^{\mathcal{A}}C^{P-D}$ controller, owing to the inherent system noise, the error fluctuates between about ±20 counts even after steady state has been reached and hence it does not satisfy the settling time criteria. Also the output shows undershoot behaviour before reaching the commanded value.

6-5 Reference tracking

The reference tracking abilities of the controllers are tested for 10 sinusoidal references with frequencies ranging from 0.1Hz upto the bandwidth of 150Hz. For sinusoidal references in linear feedback loops, one can look at the bode plots of closed loop Sensitivity ($S(j\omega)$) and Control Sensitivity ($CS(j\omega)$) to get a measure of the consequent tracking error e and control input u respectively. However, unlike the linear case where for sinusoidal inputs, the resultant signals in the loop are all sinusoids of the same frequency, in case of feedback loops with non-linear controllers, there may be higher harmonic signals as well. To capture this information, the Mechatronic System Design group at the PME departement of TU Delft, has developed two metrics on the lines of ($S(j\omega)$) and ($CS(j\omega)$) to quantify the closed loop reference tracking performance of non-linear controllers, namely pseudo-Sensitivity gain ($|S_\partial(\omega)|$) and pseudo-Control Sensitivity gain($|CS_\partial(\omega)|$). For reference $r = A_r \sin(\omega t)$, these metrics are defined as :

$$|S_\partial(\omega)| = \frac{\|e\|_\infty}{A_r} \tag{6-3}$$

$$|CS_\partial(\omega)| = \frac{\|u\|_\infty}{A_r} \tag{6-4}$$

where the $\|e\|_\infty$ and $\|u\|_\infty$ norms are computed once steady state is reached in the experiments. The $\|e\|_\infty$ in the definition of $|S_\partial(\omega)|$ captures the maximum error that can occur at steady state, which is critical information in precision applications. The $|S_\partial(\omega)|$ and $|CS_\partial(\omega)|$ plots obtained experimentally are shown in Fig. 6-9 and 6-10 respectively.

The tracking performance of the ${}^{\mathcal{A}}C^{P-I}$ controller is poorer than that of the PID controller uptil 10Hz beyond which it becomes and stays better than PID uptil about 75Hz. This performance improvement comes around the same frequency at which the 2^{nd} higher order open loop magnitude diminishes as compared to the open loop magnitude. ${}^{\mathcal{B}}C^{P-I}$ controller performs better than PID from 0.2Hz all the way upto 50Hz. The better performance of ${}^{\mathcal{B}}C^{P-I}$ as compared to ${}^{\mathcal{A}}C^{P-I}$ at frequencies below 10 Hz can be attributed to low higher order loop magnitudes. The apparent poor performance of ${}^{\mathcal{B}}C^{P-I}$ below 0.2Hz as compared to PID, can be attributed to the role of quantization and system noise which becomes noticeable at those low values of e and then plotting in dB magnifying the really small difference. A proposition that can explain the poor performance of ${}^{\mathcal{A}}C^{P-I}$ above 75Hz and ${}^{\mathcal{B}}C^{P-I}$ above 50Hz is that the tracking performance of these VFO controllers goes poorer beyond ω_c/n where n is the most dominant higher order, which is 2 for ${}^{\mathcal{A}}C^{P-I}$ and 3 for ${}^{\mathcal{B}}C^{P-I}$. Despite having the same open loop shape as ${}^{\mathcal{A}}C^{P-I}$ and higher order open loop magnitudes lower than the open loop magnitude like ${}^{\mathcal{B}}C^{P-I}$, tracking performance of the ${}^{\mathcal{A}}C^{P-D}$ controller is poorer than that of PID over the entire considered frequency range. A possible reason that

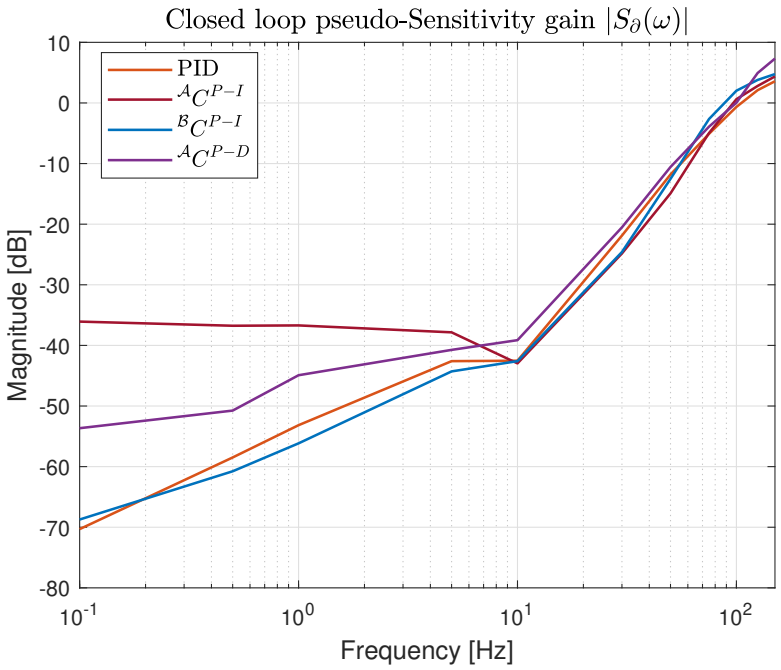

Figure 6-9: Closed loop pseudo-Sensitivity gain $|S_\partial(\omega)|$ obtained from reference tracking experiments.

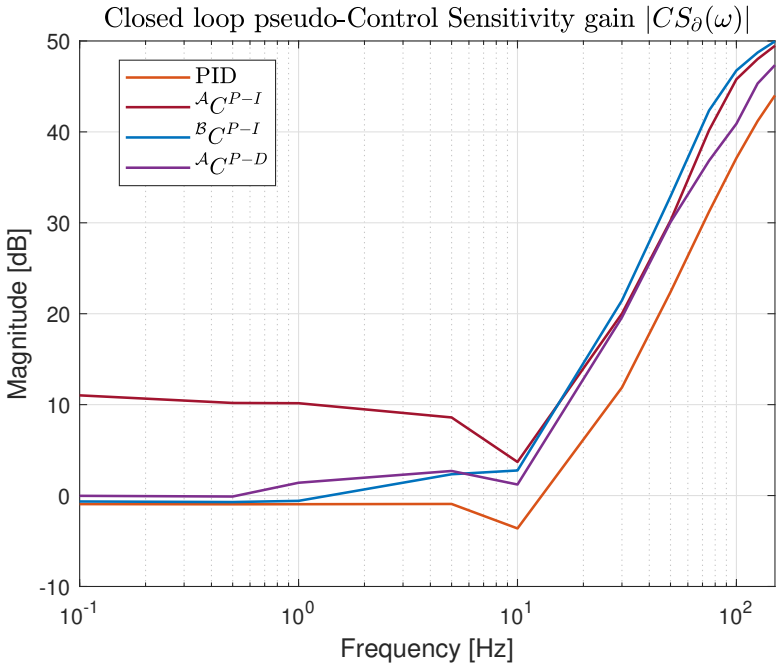

Figure 6-10: Closed loop pseudo-Control Sensitivity gain $|CS_\partial(\omega)|$ obtained from reference tracking experiments.

can explain this poor performance is that ${}^{\mathcal{A}}C^{P-D}$ controller is more susceptible to noise (as seen in Table 6-2) originating from the inherent system noise or quantization of the input.

Fig. 6-10 shows that the control action demanded by VFO controllers for tracking a given reference is more than that required by PID. Similar to the improvement in tracking performance, a reduction in the control action required by ${}^{\mathcal{A}}C^{P-I}$ is seen beyond 10Hz.

6-6 Disturbance rejection

Next, the disturbance rejection experiments for 10 disturbance signals u_d with frequencies ranging from 0.1Hz upto the bandwidth of 150Hz are performed. Similar to the $|S_\partial(\omega)|$ metric for reference tracking, we define a measure of maximum tracking error for an input disturbance signal $u_d = A_d \sin(\omega t)$ as :

$$|PS_\partial(\omega)| = \frac{\|e\|_\infty}{A_d} \tag{6-5}$$

where the $\|e\|_\infty$ norm is computed once steady state is reached in the experiments. The pseudo-Process Sensitivity $|PS_\partial(\omega)|$ plot obtained experimentally is shown in Fig. 6-11.

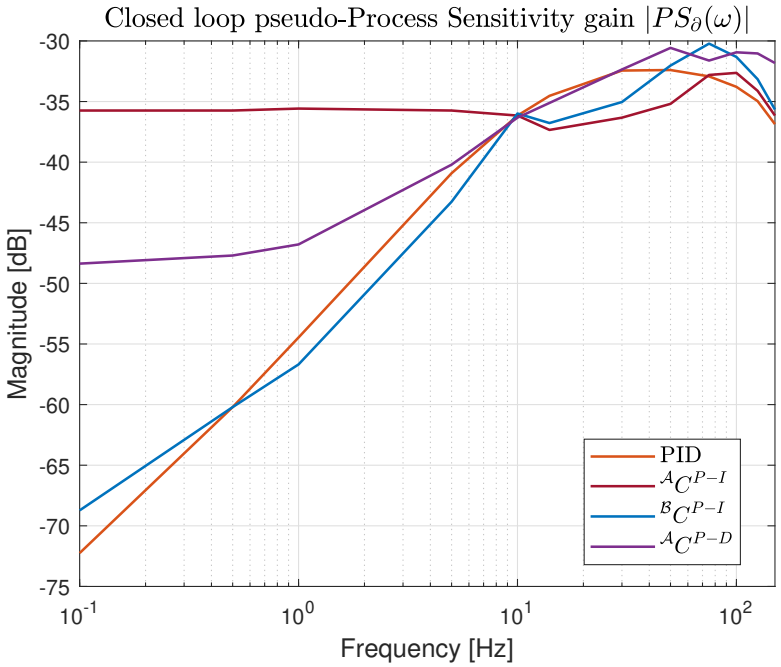

Figure 6-11: Closed loop pseudo-Process Sensitivity gain $|PS_\partial(\omega)|$ obtained from disturbance rejection experiments.

Fig. 6-11 shows that the trend in the disturbance rejection performance of these controllers is quite similar to their reference tracking performance. ${}^{\mathcal{B}}C^{P-I}$ performs better than PID at frequencies from 0.5Hz upto about 50Hz. The ${}^{\mathcal{A}}C^{P-I}$ performance improves after 10Hz and becomes and stays better than PID and ${}^{\mathcal{B}}C^{P-I}$ uptil 75 Hz. The disturbance rejection of ${}^{\mathcal{A}}C^{P-D}$ is the poorest amongst these controllers. In terms of demanded control action, it was

again observed that u_a required by VFO controllers is higher than that required by PID. The possible explanations for these characteristics of the VFO controllers are the same as those presented for explaining their reference tracking behaviour.

6-7 Discussion

Simulations showed that ${}^{\mathcal{B}}C^{P-D}$ controller is unstable. The VFO controllers show poor step responses as compared to the PID controller, despite being tuned for the same phase margin and bandwidth as PID, with the only silver lining being the lower settling time for ${}^{\mathcal{B}}C^{P-I}$ controller. Despite lower open loop gain beyond bandwidth as compared to PID, the VFO controllers are unable to attenuate noise. As suggested by the open loop shape, ${}^{\mathcal{A}}C^{P-I}$ and ${}^{\mathcal{B}}C^{P-I}$ controllers are able to provide better reference tracking and disturbance rejection performance than PID, but only in certain frequency bands and neither controller could be decisively deemed better than the other. It can be concluded that, only using the open loop shape to predict the closed loop performance of VFO controllers is inaccurate. The relatively non-trivial higher harmonics in the VFO output, which reflect in the higher order open loop magnitudes, reduce the efficacy of the purely SIDF based loop shaping.

Chapter 7

Conclusion and Recommendations

Stringent control demands from the high-tech industry have warranted the need to explore potentially advantageous non-linear controllers. VFO calculus provides one such avenue to build non-linear PID-like controllers. However, in the nascent field of VFO control, the focus has mainly been on tuning the controllers by time domain optimization of the performance for certain specific trajectories and cost functions and no work in the frequency domain can be found in literature. Frequency domain tools allow for analysis and tuning of controllers for performance over a wide range of exogenous inputs. For the smooth adoption into industry, it is important to develop a frequency domain framework for working with VFO control. This gap led us to establishing the goal of the thesis as follows :

To use DF analysis for developing VFO PID controllers in the frequency domain from an industry compatibility point of view and examining their closed loop performance in a precision positioning application.

The primary idea was to build VFO PID controllers by replacing linear filters in a rule of thumb PID controller with suitable VFO operators having an advantageous frequency response obtained using their describing function. To this end, the choices of VFO operator definitions, their implementation technique and the order switching law were made for simplicity in implementation of the operators and derivation of their describing functions. This brings us to the first contribution of the thesis, which is the analytical derivation of the describing functions, i.e., SIDF and HOSIDFs, of the VFO operators considered in the scope of this thesis. Second contribution is the development of frequency domain tuning guidelines to shape the open loop for these controllers. However, only the SIDF has been used in the loop shaping process and the HOSIDF information has been neglected, based on the critical assumption that the first harmonic content is dominant in the VFO operator output. The obtained open loop shapes suggested an improvement in closed loop performance as compared to the base PID controller. Third contribution is the experimental testing of the developed VFO controllers on a precision position stage to verify the proposed improvement in closed loop performance. Although the results were not in favour of the VFO controllers, the results helped decisively conclude that the open loop shape alone is not an accurate indicator of the closed loop performance in case of such non-linear controllers. Furthermore, on the lines

of work done for reset control systems, a preliminary analysis of the higher order open loop shapes obtained using the derived HOSIDFs was made. It was identified that the relatively non-trivial higher harmonics in the VFO output reduce the efficacy of the purely SIDF based loop shaping. This work can serve as a starting point for research into incorporating higher order information in the VFO controller tuning process.

To conclude, although the developed VFO controllers did not outperform the linear PID controller, the true objective of this thesis has been fulfilled, i.e., a preliminary framework for analysing and tuning VFO PID controllers in the frequency domain has been built. However, this work is only the first step and a lot is yet to be explored, for which there are a few recommendations as follows :

- Firstly and most importantly, a method needs to be developed to incorporate HOSIDF information into controller tuning and analysis.
- The closed loop stability of these VFO controllers is yet to be proven. Investigating multiple Lyapunov functions method or other techniques used in proving stability of switched systems can be a good starting point.
- In this thesis, only the VFO order signal $\alpha(t)$, switching between 2 orders $\alpha_1, \alpha_2 \in \{-1, 0, 1\}$ has been explored. This framework can be extended to fractional orders to capture the true essence of a VFO controller.
- In our work, only positive values have been investigated for the VFO operator gains, K_1 and K_2. However, negative gains can also be looked into, since some combinations of positive and negative gains were found to yield advantageous SIDFs.
- The current switching law can be tweaked by introducing a deadband around the switching surface or by using hysteresis switching, and the corresponding effects on the closed loop performance can be studied. Also, other complicated switching laws can be explored, that could allow switching between more than 2 orders.
- The linear filters in our VFO controllers have been obtained from a conventional PID controller. Other linear filters can be explored. Moreover, parts of the linear filter can be placed before or after the VFO operator to minimize the effect of higher order harmonics on closed loop performance, as explored for reset controllers in [39].
- On the implementation side, the effect of frequency of the pole used to make the theoretical derivative operators proper can be studied. Effect of different discretization methods and sampling frequencies can also be studied.

Appendix A

Basics and limitations of linear feedback theory

In this chapter, a short recap of loop shaping, PID control and more importantly the fundamental limitations of linear feedback control and the corresponding trade-offs is presented.

A-1 Basics of loop shaping

In this Section, some basic nomenclature and definitions, common in feedback control and loop shaping, are presented. For a detailed study, the reader is referred to [41]. Consider a Single Input Single Output (SISO) negative feedback loop as shown in Figure A-1, with a plant G being controlled by a controller C, with reference signal r[1], tracking error e, control command u, input (or load) disturbance d_u, plant output x, output disturbance d_y, actual output y, measurement no ise n_m and measured output y_m.

Here the open loop transfer function is defined as $L(s) = C(s)G(s)$. Closed loop transfer functions, namely, Complementary Sensitivity $T(s)$, Sensitivity $S(s)$, controller sensitivity $C(s)S(s)$ and plant sensitivity $G(s)S(s)$ are given as:

$$\begin{aligned} T(s) = \frac{Y(s)}{R(s)} = -\frac{U(s)}{D_u(s)} = -\frac{Y(s)}{N_m(s)} = \frac{L(s)}{1+L(s)} \\ S(s) = \frac{Y(s)}{D_y(s)} = \frac{E(s)}{R(s)} = \frac{Y_m(s)}{N_m(s)} = \frac{1}{1+L(s)} \\ C(s)S(s) = \frac{U(s)}{R(s)} = -\frac{U(s)}{N_m(s)} = -\frac{U(s)}{D_y(s)} = \frac{C(s)}{1+L(s)} \\ G(s)S(s) = \frac{Y(s)}{D_u(s)} = \frac{G(s)}{1+L(s)} \end{aligned} \tag{A-1}$$

[1]Lowercase letters like $r(t)$ represent the time domain signal while the corresponding uppercase letter, $R(s)$ represents the Laplace transform of the signal.

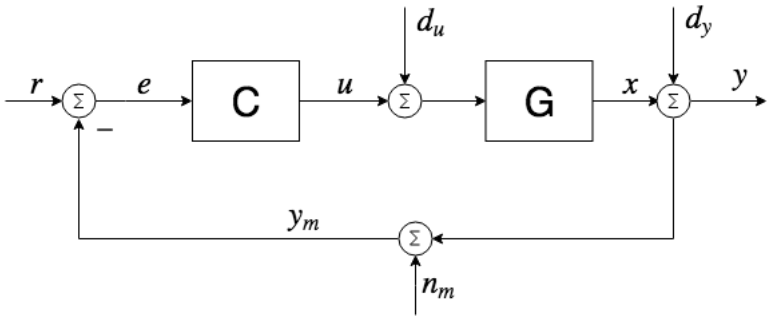

Figure A-1: A generic SISO negative feedback loop with reference signal r, tracking error e, controller C, control command u, input(or load) disturbance d_u, plant to be controlled G, plant output x, output disturbance d_y, actual output y, measurement noise n_m and measured output y_m.

Additionally, it can be seen that

$$T(s) + S(s) = 1 \tag{A-2}$$

The Laplace transform of the actual output is given as:

$$Y(s) = T(s)R(s) + S(s)D_y(s) + S(s)G(s)D_u(s) - T(s)N_m(s) \tag{A-3}$$

The Laplace transform of the actual error, $e_a = r - y$, is given as:

$$E_a(s) = S(s)R(s) - S(s)D_y(s) - S(s)G(s)D_u(s) + T(s)N_m(s) \tag{A-4}$$

The objectives of feedback control include achieving good reference tracking and disturbance rejection upto the bandwidth frequency, attenuating high frequency noise above the bandwidth and/or making the closed loop robust to model uncertainties, gain variations or time delays.

From Equation (A-4), we can see that, to achieve low error due to reference and disturbance signals, we require low $S(j\omega)$[2], thereby requiring high loop gain $L(j\omega)$ at frequencies below bandwidth. Also, to have low error due to measurement noise which exists at higher frequencies, we require low $T(j\omega)$, and thereby requiring low $L(j\omega)$ at those frequencies. Additional constraints are placed on the magnitude and phase of the loop gain, owing to requirements of stability and robustness margins like Gain, Phase and Modulus margins. Loop shaping is the technique of synthesizing the controller using frequency domain tools like Bode and Nyquist to obtain the required shape of $L(j\omega)$ thereby obtaining the desired closed loop characteristics. An ideally desired shape of $L(j\omega)$ is shown in Figure A-2.

[2]The Frequency Response Function (FRF) corresponding to a transfer function is obtained by substituting the Laplace variable s with $j\omega$. In the absence of a model, FRF may be obtained by frequency experiment data.

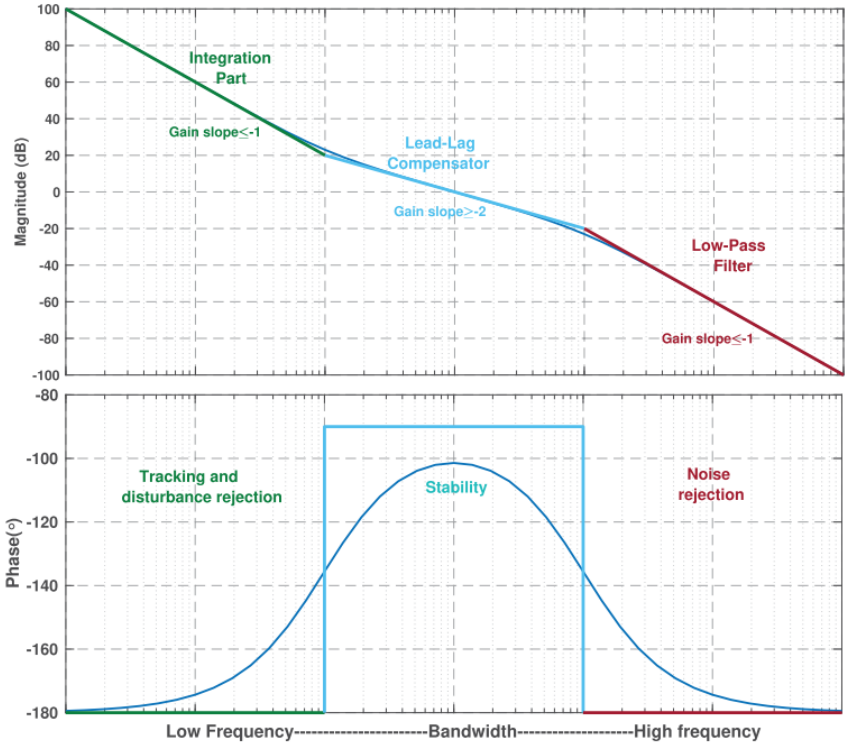

Figure A-2: Bode Plot of ideally desired loop gain in different frequency bands.(Cyan lines represent the asymptotic magnitude and phase lines, while blue lines represent the actual ones. Image courtesy [42].)

Some definitions in loop shaping:

- **Crossover frequency** ω_c is the frequency where the loop gain crosses the 0 dB magnitude. This is also one of the definitions of the closed loop bandwidth.
- **Gain Margin (GM)** is the factor by which the loop gain magnitude can be multiplied before instability occurs (i.e., loop gain becomes -1).
- **Phase Margin (PM)** is the amount of additional phase lag that can be accommodated at ω_c before instability occurs (i.e., phase of loop gain at ω_c becomes $-180\,\text{deg}$).
- **Modulus Margin (MM)** is the minimal distance between the critical point -1 and the Nyquist plot of $L(s)$. This is also the maximal peak of the Sensitivity function $S(j\omega)$ over the entire frequency range.

A-2 PID tuning : rule of thumb

An integer order PID controller in the series form:

$$C_{PID} = K_p\left(1 + \frac{\omega_i}{s}\right)\left(\frac{\frac{s}{w_d} + 1}{\frac{s}{w_t} + 1}\right) \tag{A-5}$$

where K_p is the proportional gain, ω_i is the frequency where the integrator action ends, ω_d is the frequency where the derivative action starts and ω_t is the frequency where the derivative action is tamed. The Bode plot of such a Proportional-Integral-Derivative (PID) controller is shown in Figure A-3.

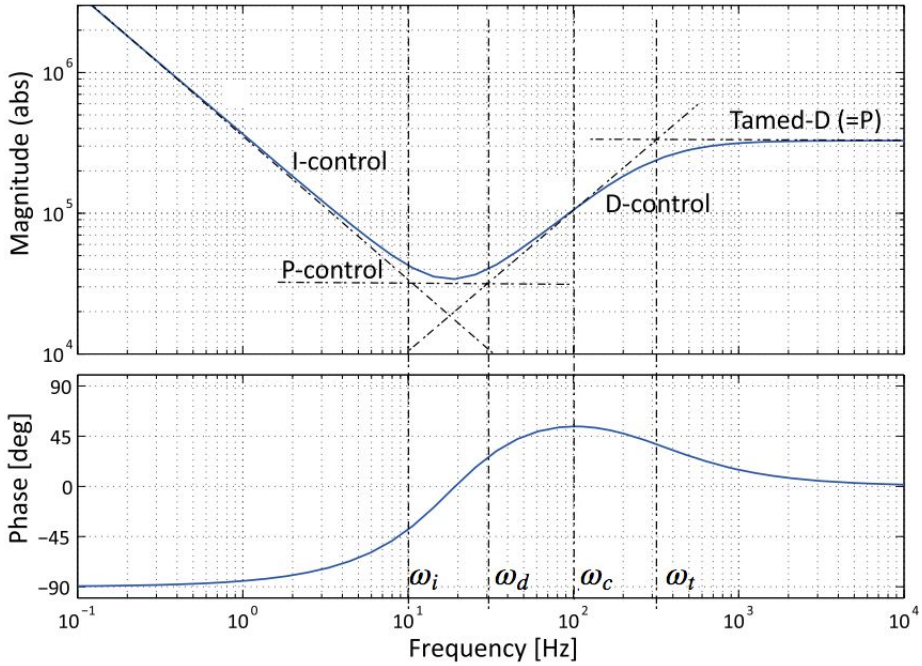

Figure A-3: Bode Plot of a generic C_{PID} controller as in Equation (A-5). (Image courtesy [40]).

The proportional action is used to control the cross over frequency. Integral action is used to remove steady state error and increase the loop gain at lower frequencies. Derivative action is used to get phase lead at the crossover frequency.

For mass based second order systems like mass, mass- spring and mass-spring-damper systems, tuning guidelines for a rule of thumb PID controller [40] are given as follows:

- To achieve unity gain at the crossover frequency, the gain of the controller, K_p must cancel the gain of the plant at ω_c ($|G|_{\omega_c}$). Also, K_p must cancel the additional gain introduced by the derivative action depending on the ratio of ω_c and ω_d as will be discussed ahead.
  $K_p = \frac{\omega_d/\omega_c}{|G|_{\omega_c}} = \frac{0.33}{|G|_{\omega_c}}$

- The derivative action should start at a frequency one third of ω_c so that phase starts increasing well before ω_c and a substantial phase margin can be achieved. $\omega_d = 0.33\omega_c$.

- The derivative action should be terminated at a frequency beyond ω_c so as not to amplify noise at higher frequencies, this is done at three times of ω_c. $\omega_t = 3\omega_c$. It must be noted that keeping ω_t and ω_d geometrically symmetric about ω_c helps achieve maximum phase lead exactly at ω_c and not before or after it.

- The integrator action, starting from very low frequencies should stop at a frequency one third of ω_d so that the $\pi/2\ rad$ phase lag caused by the integrator can be fully recovered before ω_c. Thus $\omega_i = 0.33\omega_d \approx 0.1\omega_c$.

This rule of thumb PID controller when applied to mass based second order plants can achieve a phase margin of about 45 deg and bound the maximum peaks of Sensitivity and Complementary Sensitivity to under $3\,dB$.

A-3 Limitations and trade-offs in linear control

Achievable performance by using linear feedback control has fundamental limitations [4,5,43].

A-3-1 Bode's gain phase relationship

For a stable minimum phase system(i.e., all the poles and zeros in the left half plane) $G(s)$, a unique relation exists between the magnitude $|\cdot|$ and phase $\angle$ of its FRF $G(j\omega)$. Bode's gain phase relation states that at a frequency ω_0,

$$\begin{aligned}\angle G(j\omega_0) &= \frac{1}{\pi}\int_0^\infty \frac{d\log|G(j\omega)|}{d\log(\omega)}\log\left|\frac{\omega+\omega_0}{\omega-\omega_0}\right| d\log(\omega)\\ &= \frac{\pi}{2}\int_0^\infty f(\omega)\frac{d\log|G(j\omega)|}{d\log(\omega)}d\log(\omega)\end{aligned} \tag{A-6}$$

where the weighting kernel $f(\omega)$ is given as,

$$f(\omega) = \frac{2}{\pi^2}\log\left|\frac{\omega+\omega_0}{\omega-\omega_0}\right| = \frac{2}{\pi^2}\log\left|\frac{\frac{\omega}{\omega_0}+1}{\frac{\omega}{\omega_0}-1}\right|$$

$f(\omega)$ practically dies out beyond a decade above and below the frequency of interest ω_0. Thus for a slope that remains constant over this interval, (A-6) can be approximated to:

$$\angle G(j\omega_0) = \frac{\pi}{2}\frac{d\log|G(j\omega)|}{d\log(\omega)} = \frac{\pi}{2}n$$

where for eg. $n = -1$ for a slope of $-20\,dB/dec$ in the Bode plot and $n = +2$ for a slope of $+40\,dB/dec$.

To understand trade-off arising from Bode's gain phase relation, let us consider a PID controller as given in Equation (A-5) and designed[3] for a crossover frequency ω_c of 100 Hz. From Figure A-4a, it can be seen that such a controller provides a phase of around 50 deg at ω_c. Suppose an additional D-action is employed, i.e., a PID^2 controller, to achieve higher phase at ω_c, then this is accompanied by an inevitable additional magnitude slope of +20 dB/dec,

[3]The corresponding gains for the controller can be obtained using rule of thumb guidelines presented in Section A-2

thereby amplifying the noise at higher frequencies and reducing gain magnitude at lower frequencies, i.e., deteriorating reference tracking and disturbance rejection, as compared to the PID. This can be seen in Figure A-4a.

$$PID = \frac{1}{3|G|_{\omega_c}}\left(1+\frac{\omega_c}{10s}\right)\left(\frac{\frac{3s}{\omega_c}+1}{\frac{s}{3\omega_c}+1}\right) \qquad PID^2 = \frac{1}{9|G|_{\omega_c}}\left(1+\frac{\omega_c}{10s}\right)\left(\frac{\frac{3s}{\omega_c}+1}{\frac{s}{3\omega_c}+1}\right)^2$$

While on the other hand, to achieve higher loop gain at lower frequencies, if an additional integral action is employed, i.e., a PI^2D controller, then this comes with extra phase lag, leading to a slight reduction in phase at ω_c (Figure A-4b) which deteriorates transient response in terms of increased overshoot and settling times.

$$PI^2D = \frac{1}{3|G|_{\omega_c}}\left(1+\frac{\omega_c}{10s}\right)^2\left(\frac{\frac{3s}{\omega_c}+1}{\frac{s}{3\omega_C}+1}\right)$$

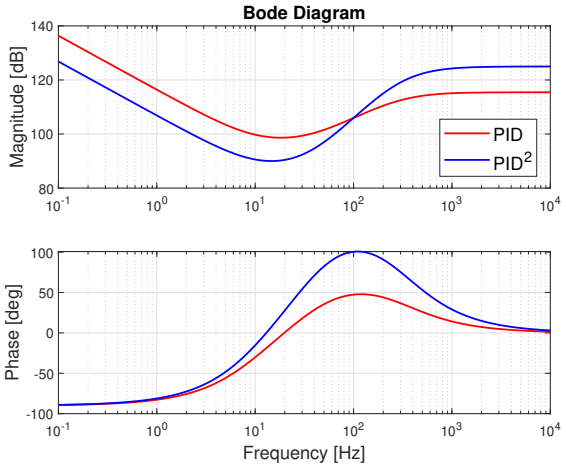

(a) Bode plot of PID and PID^2 controllers

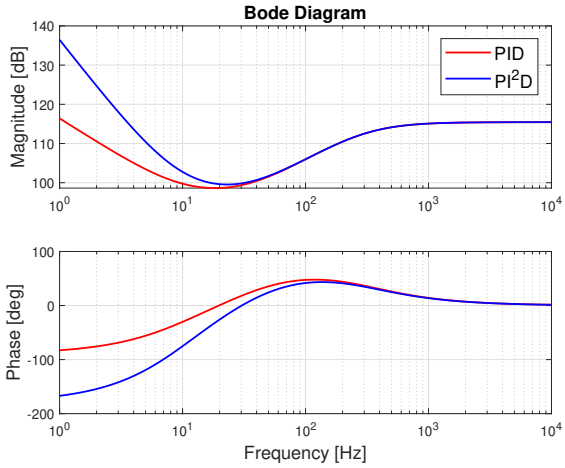

(b) Bode plot of PID and PI^2D controllers

Figure A-4: Bode plots comparing PID^2, PI^2D and PID controllers to demonstrate Bode gain phase relationship

A-3-2 Waterbed effect

Bode's Sensitivity integral is given by

$$\int_0^\infty \ln|S(j\omega)|d\omega = \pi\sum_k Re(p_k) - \frac{\pi}{2}\lim_{s\to\infty} sL(s)$$

where p_k are the right half plane poles of $L(s)$. In the absence of right half plane poles and when the relative degree of $L(s) \geq 2$, then this integral simplifies to

$$\int_0^\infty \ln|S(j\omega)|d\omega = 0$$

This integral translates to a push-pop effect, i.e., if we reduce the magnitude of $S(j\omega)$ at some frequency then it increases at other frequencies. To understand the trade-off let us consider a pure mass system $G = \frac{1}{0.5s^2}$. Consider two different PID controllers C_1 and C_2 designed for a ω_c of $2\pi 100\ rad/s$.

$$C_1 = \frac{1}{3|G|_{\omega_c}}\left(1 + \frac{\omega_c}{10s}\right)\left(\frac{\frac{3s}{\omega_c} + 1}{\frac{s}{3\omega_C} + 1}\right) \qquad C_2 = \frac{1}{8|G|_{\omega_c}}\left(1 + \frac{\omega_c}{10s}\right)\left(\frac{\frac{8s}{\omega_c} + 1}{\frac{s}{8\omega_C} + 1}\right)$$

Controller C_2 is designed such that it achieves higher PM and flatter phase around ω_c thus making the closed loop more robust to gain variations as compared to C_1. The corresponding open loop transfer functions are $L_1(s), L_2(s)$ and the corresponding Bode plots are given in Fig. A-5a and the sensitivity functions are $S_1(s), S_2(s)$. Though C_2 pushes the maximum peak of $S_2(s)$ to lower than that of $S_1(s)$, the magnitude of $S_2(s)$ over the entire range of low frequencies becomes more than that of $S_1(s)$ (Fig. A-5b), thereby adversely affecting reference tracking and disturbance rejection. This is the classic performance robustness trade-off.

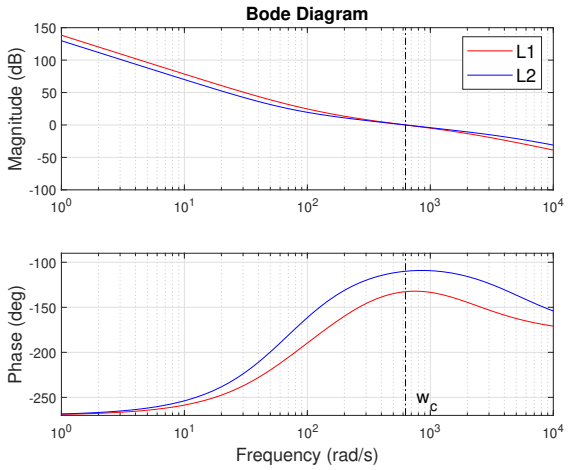

(a) Bode plot of open loop transfer functions $L_1(s)$ and $L_2(s)$.

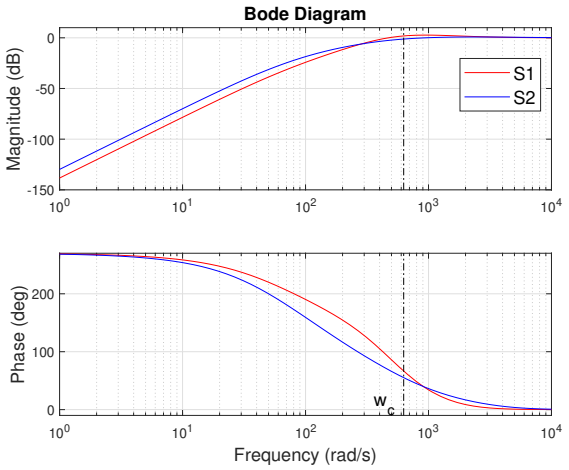

(b) Bode plot of Sensitivity transfer functions $S_1(s)$ and $S_2(s)$.

Figure A-5: Bode plots comparing the loop transfer functions and Sensitivity functions for two different controllers to demonstrate waterbed effect.

Bibliography

[1] H. Butler, "Position control in lithographic equipment," *IEEE Control Systems Magazine*, vol. 31, no. 5, pp. 28–47, 2011.

[2] M. Iwasaki, K. Seki, and Y. Maeda, "High-precision motion control techniques: A promising approach to improving motion performance," *IEEE Industrial Electronics Magazine*, vol. 6, no. 1, pp. 32–40, 2012.

[3] M. Steinbuch and M. L. Norg, "Advanced motion control: An industrial perspective," *European Journal of Control*, vol. 4, no. 4, pp. 278–293, 1998.

[4] G. Stein, "Respect the unstable," *IEEE Control Systems Magazine*, vol. 23, no. 4, pp. 12–25, 2003.

[5] K. J. Åström, "Limitations on control system performance," *European Journal of Control*, vol. 6, no. 1, pp. 2–20, 2000.

[6] J. Sabatier, P. Melchior, A. Oustaloup, and P. Lanusse, "Fractional order differentiation and robust control design: Crone, h-infinity and motion control," 2015.

[7] I. Podlubny, "Fractional-order systems and pi/sup/spl lambda//d/sup/spl mu//-controllers," *IEEE Transactions on automatic control*, vol. 44, no. 1, pp. 208–214, 1999.

[8] W. Foster, D. Gieseking, and W. Waymeyer, "A nonlinear filter for independent gain and phase (with applications)," *Journal of Basic Engineering*, vol. 88, no. 2, pp. 457–462, 1966.

[9] J. Clegg, "A nonlinear integrator for servomechanisms," *Transactions of the American Institute of Electrical Engineers, Part II: Applications and Industry*, vol. 77, no. 1, pp. 41–42, 1958.

[10] N. Saikumar, R. Sinha, and S. H. Hoseinnia, "'constant in gain lead in phase'element-application in precision motion control," *IEEE/ASME Transactions on Mechatronics*, 2019.

[11] L. Zaccarian, D. Nesic, and A. R. Teel, "First order reset elements and the clegg integrator revisited," in *Proceedings of the 2005, American Control Conference, 2005.*, pp. 563–568, IEEE, 2005.

[12] L. Hazeleger, M. Heertjes, and H. Nijmeijer, "Second-order reset elements for stage control design," in *2016 American Control Conference (ACC)*, pp. 2643–2648, IEEE, 2016.

[13] I. Boiko, "Variable-structure pid controller for level process," *Control Engineering Practice*, vol. 21, no. 5, pp. 700–707, 2013.

[14] J.-J. E. Slotine, W. Li, *et al.*, *Applied nonlinear control*, vol. 199. Prentice hall Englewood Cliffs, NJ, 1991.

[15] C. Lorenzo and T. Hartley, "Variable fractional order and distributed order operators," *Nonlinear Dyn*, vol. 29, pp. 57–98, 2002.

[16] C. F. Coimbra, "Mechanics with variable-order differential operators," *Annalen der Physik*, vol. 12, no. 11-12, pp. 692–703, 2003.

[17] J. P. Neto, R. M. Coelho, D. Valério, S. Vinga, D. Sierociuk, W. Malesza, M. Macias, and A. Dzieliński, "Variable order differential models of bone remodelling," *IFAC-PapersOnLine*, vol. 50, no. 1, pp. 8066–8071, 2017.

[18] D. Sierociuk and M. S. Wiraszka, "A New Variable Fractional-Order PI Algorithm $*$," *IFAC-PapersOnLine*, vol. 51, no. 4, pp. 745–750, 2018.

[19] D. Sierociuk and M. Macias, "Comparison of variable fractional order pid controller for different types of variable order derivatives," in *Proceedings of the 14th International Carpathian Control Conference (ICCC)*, pp. 334–339, IEEE, 2013.

[20] A. Dabiri, B. P. Moghaddam, and J. A. Machado, "Optimal variable-order fractional PID controllers for dynamical systems," *Journal of Computational and Applied Mathematics*, vol. 339, pp. 40–48, 2018.

[21] C. A. Monje, Y. Chen, B. M. Vinagre, D. Xue, and V. Feliu-Batlle, *Fractional-order systems and controls: fundamentals and applications*. Springer Science & Business Media, 2010.

[22] J. T. Machado, "And i say to myself:"what a fractional world!"," *Fractional Calculus and Applied Analysis*, vol. 14, no. 4, pp. 635–654, 2011.

[23] H. Sheng, H. G. Sun, C. Coopmans, Y. Q. Chen, and G. W. Bohannan, "A Physical experimental study of variable-order fractional integrator and differentiator," vol. 104, pp. 93–104, 2011.

[24] D. Valério and J. S. Da Costa, "Variable-order fractional derivatives and their numerical approximations," *Signal Processing*, vol. 91, no. 3, pp. 470–483, 2011.

[25] D. Sierociuk, W. Malesza, and M. Macias, "On the recursive fractional variable-order derivative: equivalent switching strategy, duality, and analog modeling," *Circuits, Systems, and Signal Processing*, vol. 34, no. 4, pp. 1077–1113, 2015.

[26] D. Sierociuk, W. Malesza, and M. Macias, "Derivation, interpretation, and analog modelling of fractional variable order derivative definition," *Applied Mathematical Modelling*, vol. 39, no. 13, pp. 3876–3888, 2015.

[27] D. Sierociuk, W. Malesza, and M. Macias, "On a new definition of fractional variable-order derivative," in *Proceedings of the 14th International Carpathian Control Conference (ICCC)*, pp. 340–345, IEEE, 2013.

[28] M. Macias and D. Sierociuk, "An alternative recursive fractional variable-order derivative definition and its analog validation," in *ICFDA'14 International Conference on Fractional Differentiation and Its Applications 2014*, pp. 1–6, IEEE, 2014.

[29] M. Macias, *Fractional Variable-Order Models of particular dynamical systems.* PhD thesis, Warsaw University of Technology, 2018.

[30] D. Sierociuk, "Fractional variable order derivative simulink toolkit," *Online](Matlab Central) http://www. mathworks. com/matlabcentral/fileexchange/38801*, 2012.

[31] D. Valério, G. Vinagre, J. Domingues, and J. Sá da Costa, "Variable-Order Fractional Derivatives and Their Numerical Approximations I - Real Orders," *Symposium on Fractional Signals and Systems*, pp. 1–13, 2009.

[32] A. Oustaloup, F. Levron, B. Mathieu, and F. M. Nanot, "Frequency-band complex noninteger differentiator: characterization and synthesis," *IEEE Transactions on Circuits and Systems I: Fundamental Theory and Applications*, vol. 47, no. 1, pp. 25–39, 2000.

[33] P. Ostalczyk, "Variable-, fractional-order discrete PID controllers," *2012 17th International Conference on Methods and Models in Automation and Robotics, MMAR 2012*, pp. 534–539, 2012.

[34] A. Gelb and W. E. Van der Velde, *Multiple-input describing functions and non-linear system design.* McGraw-Hill electronic sciences series, New York, NY: McGraw-Hill, 1968.

[35] P. Nuij, O. Bosgra, and M. Steinbuch, "Higher-order sinusoidal input describing functions for the analysis of non-linear systems with harmonic responses," *Mechanical Systems and Signal Processing*, vol. 20, no. 8, pp. 1883–1904, 2006.

[36] P. Nuij, *Higher order sinusoidal input describing functions - Extending linear techniques towards non-linear systems analysis.* PhD thesis, TU Eindhoven, 2007.

[37] K. Heinen, "Frequency analysis of reset systems containing a clegg integrator: An introduction to higher order sinusoidal input describing functions," 2018.

[38] Y. Salman, "Tuning a novel reset element through describing function and hosidf analysis," 2018.

[39] C. Cai, "The optimal sequence for reset controllers," 2019.

[40] R. M. Schmidt, G. Schitter, and A. Rankers, *The Design of High Performance Mechatronics-: High-Tech Functionality by Multidisciplinary System Integration.* Ios Press, 2014.

[41] S. Skogestad and I. Postlethwaite, *Multivariable Feedback Control: Analysis and Design*. John Wiley & Sons, Inc., 2005.

[42] A. A. Dastjerdi, N. Saikumar, and S. H. HosseinNia, "Tuning guidelines for fractional order PID controllers: Rules of thumb," *Mechatronics*, vol. 56, no. October, pp. 26–36, 2018.

[43] M. Seron, J. Braslavsky, and G. Goodwin, *Fundamental limitations in filtering and control*. 2012.